Available online at www.sciencedirect.com
ScienceDirect
Journal of Computational Physics 227 (2008) 6795–6820
JOURNAL OF COMPUTATIONAL PHYSICS
www.elsevier.com/locate/jcp

Dissipative terms and local time-stepping improvements in a spatial high order Discontinuous Galerkin scheme for the time-domain Maxwell's equations

E. Montseny [a], S. Pernet [b,*], X. Ferriéres [c], G. Cohen [d]

[a] ONERA, LAAS-CNRS, University of Toulouse, 7 Av. du Colonel Roche, 31077 Toulouse, France
[b] CERFACS, 42 Avenue Gaspard Coriolis, 31507 Toulouse, France
[c] ONERA, 2 Avenue Edouard Belin, 31055 Toulouse, France
[d] INRIA, Domaine de Voluceau, BP-105 Rocquencourt, Le Chesnay Cedex, France

Received 26 April 2007; received in revised form 21 March 2008; accepted 25 March 2008
Available online 4 April 2008

Abstract

In this paper, we present some improvements, in terms of accuracy and speed-up, for a particular well adapted Discontinuous Galerkin method devoted to the time-domain Maxwell equations. First, to reduce spurious modes on very distorted meshes, the addition of dissipative terms as penalization in the numerical scheme is studied and compared on examples. Second, in order to increase the efficiency of the method, a multi-class local time-stepping strategy is presented and its validation and advantages are highlighted on different examples.

Keywords: Maxwell's equations; Discontinuous Galerkin method; Local time-stepping

1. Introduction

In order to limit dispersive and dissipative errors [1] generated by classical schemes used to solve the time-domain Maxwell equations like FDTD [2,3] or FVTD [4–6], some other methods as Discontinuous Galerkin (DG) methods [7], using high order spatial approximation of the fields in each cell, have been studied. Such methods are generally used with unstructured meshes and naturally allow spatial refinements when necessary, as for example near walls or in presence of materials with high dielectric contrasts. We have developed for the Maxwell equations a DG method based on a leap-frog scheme in time and a non-dissipative fluxes formulation [8]. However, the use of unstructured meshes can imply the presence of very distorted and small cells. Consequently, to ensure accuracy and stability, an increase of the spatial order and small time steps are required in the current available scheme. In this paper, after a first section in which we recall the principles and advantages

* Corresponding author.
E-mail address: pernet@cerfacs.fr (S. Pernet).

0021-9991/$ - see front matter © 2008 Elsevier Inc. All rights reserved.
doi:10.1016/j.jcp.2008.03.032

of the particular DG method under consideration, we study in the second section the way to reduce spurious modes, and then the way to increase accuracy by introducing a penalization of the fluxes by dissipative terms. In particular, via a mathematical analysis, we show the convergence of the scheme even when using an order 1 spatial approximation, which is not the case without those dissipative terms [10]. Finally, in a third section, we develop a multi-class local time-stepping strategy adapted to the leap-frog time scheme classically used for Maxwell's equations [2]. The efficiency of this approach is compared with various local time-stepping strategies in terms of reduction of CPU time. Some validations on examples are given, in particular the possibility of using this local time-stepping method on cavity problems is emphasized.

2. Principles and advantages of the Discontinuous Galerkin method considered

Let Ω be a bounded open subset of $\mathbb{R}^3$ whose boundary is $\partial\Omega$, and let n denotes the unit outward normal to Ω. Let $\varepsilon(x)$, $\mu(x)$ and $\sigma(x)$ denote, respectively, the permittivity, the permeability and the conductivity of the medium.We consider the problem described by the Maxwell equations:

Find $(E,H):\Omega\times]0,T[\to\mathbb{R}^3\times\mathbb{R}^3$ such that:

$$\begin{cases}\varepsilon\partial_t E+\sigma E=\nabla\times H,\\ \mu\partial_t H=-\nabla\times E,\\ n\times E=0\quad\text{on }\partial\Omega.\end{cases}\tag{1}$$

where E and H define the electric and magnetic fields. The boundary condition is not restrictive because it is used both to treat closed problems as cavity and to bound the Perfectly Matched Layers (PML) domain [11].

Consider a set $\mathcal{T}$ of hexahedral elements $(K_i)_{i=1\ldots N}$ being a partition of Ω. We introduce the following approximate space:

$$\mathbf{V}_r=\{\mathbf{v}\in[L^2(\Omega)]^3;\forall K\in\mathcal{T},DF_K^*\mathbf{v}|_K\circ F_K\in[Q_r(\widehat{K})]^3\},\tag{2}$$

where $\widehat{K}=[0,1]^3$ is the unit cube, $\forall K\in\mathcal{T}$, $F_K:\widehat{K}\to K$ denotes the trilinear mapping which associates the vertices of each element, $Q_r(\widehat{K})$ is the space of polynomials of degree at most equal to $r\in\mathbb{N}^*$ in each variable on $\widehat{K}$ and DF_K and J_K are, respectively, the Jacobian matrix and its determinant associated with the map F_K. Moreover, to each $K\in\mathcal{T}$, we associate the outward unit normal n_K.

Usually, for DG methods, E and H fields are approximated by polynomials on each cell. In our case, we approximate by polynomials the fields $DF_K^*E\circ F_K$ and $DF_K^*H\circ F_K$ on $\widehat{K}$. It is not a strange choice since the Jacobian matrix is the essential ingredient to build a conform H-curl approximation [12]. As we shall see it later, this will imply interesting properties for memory storage.

Finally, we consider the following semi-discrete DG method:find $(E_h(\cdot,t),H_h(\cdot,t))\in\mathbf{V}_r\times\mathbf{V}_r$ such that : $\forall K\in\mathcal{T}$ and $\forall\ \psi,\ \phi\in\mathbf{V}_r$

$$\begin{cases}\int_K\varepsilon\partial_t E_h\cdot\psi\,\mathrm{d}x+\int_K\sigma E_h\cdot\psi\,\mathrm{d}x=\int_K\nabla\times H_h\cdot\psi\,\mathrm{d}x+\int_{\partial K}\left(\alpha_{\partial K}^K[\![n_K\times(E_h\times n_K)]\!]_{\partial K}^K\right.\\ \quad\left.+\beta_{\partial K}^K[\![H_h\times n_K]\!]_{\partial K}^K\right)\cdot\psi\,\mathrm{d}s,\\ \int_K\mu\partial_t H_h\cdot\phi\,\mathrm{d}x=-\int_K\nabla\times E_h\cdot\phi\,\mathrm{d}x+\int_{\partial K}\left(\gamma_{\partial K}^K[\![E_h\times n_K]\!]_{\partial K}^K+\delta_{\partial K}^K[\![n_K\times(H_h\times n_K)]\!]_{\partial K}^K\right)\cdot\phi\,\mathrm{d}s,\end{cases}\tag{3}$$

where $\alpha_{\partial K}^K$, $\beta_{\partial K}^K$, $\gamma_{\partial K}^K$, $\delta_{\partial K}^K$ are parameters constant per face and $[\![v]\!]_\Gamma^K=(v|_{K'})_\Gamma-(v|_K)_\Gamma$ the jump across the boundary $\Gamma=K'\cap K$. When Γ is a boundary face (ie $\Gamma=K\cap\partial\Omega$) then K' does not exist and we simply define $[\![v]\!]_\Gamma^K=-(v|_K)_\Gamma$.

The coefficients $\alpha_{\partial K}^K$, $\beta_{\partial K}^K$, $\gamma_{\partial K}^K$, $\delta_{\partial K}^K$ are chosen such that (1) and (3) are equivalent problems (in the continuous sense) and to ensure a conservative formulation:

- $\forall\ \Gamma=K\cap K'$, $\alpha_\Gamma^K=\alpha_\Gamma^{K'}=0$, $\delta_\Gamma^K=\delta_\Gamma^{K'}=0$, $\beta_\Gamma^K=\beta_\Gamma^{K'}=-\frac{1}{2}$, $\gamma_\Gamma^K=\gamma_\Gamma^{K'}=\frac{1}{2}$.
- $\forall\ \Gamma=K\cap\partial\Omega$, $\beta_\Gamma^K=0=\delta_\Gamma^K=\alpha_\Gamma^K$, $\gamma_\Gamma^K=1$.

For the time discretization, as for the FDTD method, we use a Leap-Frog numerical scheme where the electric fields are evaluated at the time $n\Delta t$ and the magnetic fields at the time $(n+\frac{1}{2})\Delta t$, with Δt the time step and n the current iteration.

In order to define a set $\mathcal{B}$ of basis functions of $\mathbf{V}_r$, we first define a set $\widehat{\mathcal{B}}$ of basis functions of $\widehat{K}$. Let $\hat{\mathbf{x}}_{ijk} = (\hat{x}_i, \hat{y}_j, \hat{z}_k)$, $1 \leqslant i, j, k \leqslant r+1$ be a set of points of $\widehat{K}$, where $\hat{x}_i$, $\hat{y}_j$ and $\hat{z}_k$ are Gauss quadrature points on $[0,1]$. At the point $\hat{\mathbf{x}}_{ijk}$, we define on $\widehat{K}$ three basis functions $\hat{\varphi}^l_{ijk}(\hat{x},\hat{y},\hat{z}) = L_i(\hat{x})L_j(\hat{y})L_k(\hat{z})e^l$ where $L_i(\hat{x}) = \frac{\prod_{m=1,m\neq i}^{r+1}(\hat{x}-\hat{x}_m)}{\prod_{m=1,m\neq i}^{r+1}(\hat{x}_i-\hat{x}_m)}$ is the Lagrange interpolation polynomial and $(e^l)_{l=1,2,3}$ denotes the classical Cartesian base. On $K \in \mathcal{T}$, the corresponding basis functions are defined by $\varphi^{l,K}_{ijk} \circ F_K(\hat{\mathbf{x}}) = (DF^*_K)^{-1}\hat{\varphi}^l_{ijk}(\hat{\mathbf{x}})$ where $\hat{\mathbf{x}} = (\hat{x},\hat{y},\hat{z})$. Finally, the set of basis function of $\mathbf{V}_r$ is

$$\mathcal{B} = \{\varphi^{l,K}_{ijk} : K \in \mathcal{T},\ l = 1,2,3 \text{ and } i,j,k = 1,\cdots,r+1\}$$

and the dimension of $\mathbf{V}_r$ is $3(r+1)^3N$ (where N is the number of cells). So, each $U(\cdot,t) \in \mathbf{V}_r$ can be written in this way: $\forall K \in \mathcal{T}$

$$U_{|K}(\mathbf{x},t) = \sum_{l=1}^{3}\sum_{ijk=1}^{r+1} U(t)^{l,K}_{ijk}\varphi^{l,K}_{ijk}(\mathbf{x}),$$

where $U(t)^{l,K}_{ijk} \in \mathbb{R}$ is the degree of freedom associated to the basis function $\varphi^{l,K}_{ijk}$.

In the sequel, we say the DG method is a $\mathcal{Q}_r$ approximation when we choose a spatial approximation order of r. Thanks to the chosen approximation space, we have: $\forall K \in \mathcal{T}$, $l,s = 1,2,3$ and $i,j,k,m,n,p = 1,\ldots,r+1$

$$\begin{cases} \int_K (\nabla \times \varphi^{l,K}_{ijk}) \cdot \varphi^{s,K}_{mnp}\,\mathrm{d}x = \mathrm{sign}(J_K)\int_{\widehat{K}} (\hat{\nabla} \times \hat{\varphi}^l_{ijk}) \cdot \hat{\varphi}^s_{mnp}\,\mathrm{d}\hat{x} \\ \int_{\partial K} (\varphi^{l,K}_{ijk} \times n_K) \cdot \varphi^{s,K}_{mnp}\,\mathrm{d}s = \mathrm{sign}(J_K)\int_{\partial\widehat{K}} (\hat{\varphi}^l_{ijk} \times \hat{n}) \cdot \hat{\varphi}^s_{mnp}\,\mathrm{d}\hat{s}, \end{cases} \tag{4}$$

where $\hat{n}$ is the outward unit normal to $\widehat{K}$.

By using Eq. (4) and a Gauss quadrature rule to evaluate integrals, we obtain:

– For Mass matrices, $((M)_{pl}$ denotes the (p,l) component of the matrix $M)$:

$$\int_K \varepsilon U \cdot \varphi^{l,K}_{ijk}\,\mathrm{d}x = \omega_{ijk}\sum_{p=1}^{3} U^{p,K}_{ijk}|J_K|(DF_K^{-1}(\varepsilon \circ F_K)DF_K^{*-1})_{pl}(\hat{x}_{ijk}).$$

– For Stiffness matrices, $((M)_l$ denotes the component l of vector $M)$:

$$\int_K \nabla \times U \cdot \varphi^{l,K}_{ijk} = \mathrm{sign}(J_K)\sum_{mnq=1}^{r+1}\sum_{p=1}^{3} \omega_{ijk}U^{l,K}_{ijk}(\hat{\nabla} \times \hat{\varphi}^m_{ijk}(\hat{x}_{ijk}))_l.$$

– For Jump matrices:

$$\begin{aligned} \int_{\partial K} [\![H \times n_K]\!]_{\partial K} \cdot \varphi^{l,K}_{ijk}\,\mathrm{d}s = &-\mathrm{sign}(J_{K'})\int_{\partial\widehat{K}} (DF_K^{-1} \circ S_{K'K}DF_{K'})(\widehat{H}_{K'} \times \hat{n}) \cdot \hat{\varphi}^l_{ijk} \circ S_{K'K}\,\mathrm{d}\hat{s} \\ &+ \mathrm{sign}(J_K)\int_{\partial\widehat{K}} (\widehat{H}_K \times \hat{n}) \cdot \hat{\varphi}^l_{ijk}\,\mathrm{d}\hat{s}. \end{aligned}$$

In the above expressions ω_{ijk} is the quadrature weight at point $\hat{x}_{ijk}$ and $S_{K'K} = F_K^{-1} \circ F_{K'}$. $DF_K^{-1} \circ S_{K'K}DF_{K'}$ is a permutation matrix constant per face (see [8] for more detail).

The DG formulation (3) finally leads to:

$$\begin{cases} M_\varepsilon \partial_t E + M_\sigma E = RH - S^i H, \\ M_\mu \partial_t H = -RE + S^i E + S^b E, \end{cases} \tag{5}$$

where M_ε, M_μ and M_σ are 3×3 block-diagonal matrices, R the stiffness matrix, S^i and S^b are jump matrices. Thanks to the choice of approximation space and basis functions, only the mass matrix has to be stored because of its dependence on the cells K. Stiffness and jump matrices just require to store the sign of the Jacobians J_K and some computations made on the reference element $\widehat{K}$.

The important advantage of this DG method is to give, regardless of the space approximation order, a very low memory storage and a small cost of computation to evaluate the matrices of the numerical scheme. This allows us to use meshes with a small number of cells and a high order spatial approximation to obtain very accurate solutions. Consequently, the memory and CPU costs are lower than for methods based on an order 2 spatial approximation using more refined meshes. In fact, high order spatial approximation and unstructured meshes reduce the dispersive and dissipative errors of the scheme, and improve the accuracy near the structures compared to staircase methods such as FDTD. Therefore the proposed method is well-adapted to electromagnetic compatibility (EMC) problems for which it is essential to know the fields near the structures, but also to cavity problems where the dispersive and dissipative errors cannot be neglected.

To illustrate these advantages, we consider the propagation of a mode inside a perfectly metallic cavity with an edge length equal to 1 m. We study the propagative mode $(3,0,0)$, whose analytical solution is given by:

$$\begin{cases} E_x = E_y = H_z = 0 \\ E_z = \sin(3\pi(x - x_0))\sin(3\pi(y - y_0))\cos(\omega t) \\ H_x = \frac{3\pi}{\omega\mu_0} sin(3\pi(x - x_0))\cos(3\pi(y - y_0))\sin(\omega t) \\ H_y = \frac{3\pi}{\omega\mu_0}\cos(3\pi(x - x_0))\sin(3\pi(y - y_0))\sin(\omega t) \end{cases}$$

with $\omega = c_0 3\pi\sqrt{2}$ and (x_0, y_0, z_0) the center of the cavity. In Fig. 1 and Table 1, we can compare results obtained with the FDTD and DG methods. The improvement is expressed in terms of storage and CPU time. In this example, with a high spatial approximation (Q_6) with the DG method, only $3 \times 3 \times 3$ Cartesian cells have been required to mesh the cavity.

Other examples have been treated in [8] and show the advantages of this DG method for EM scattering problems.

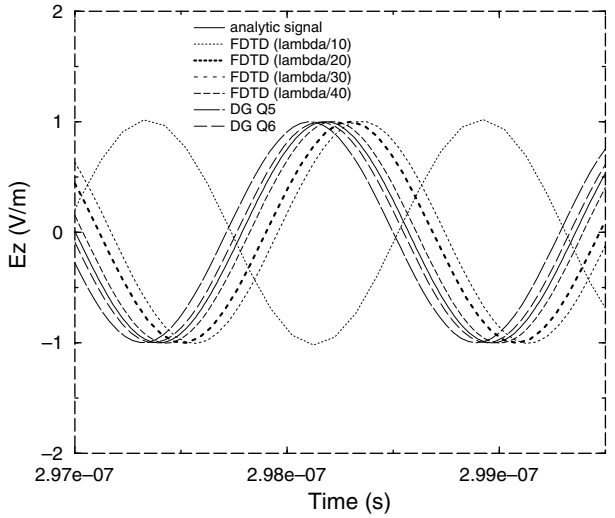

Fig. 1. Comparison of FDTD/DG results at the center of the cavity.

Table 1
Memory and CPU time costs

Method	FDTD $\lambda/10$	FDTD $\lambda/20$	FDTD $\lambda/30$	FDTD $\lambda/40$	DG Q5	DG Q6
CPU time (s)	40	120	300	840	257	490
Memory (MBytes)	1.5	5	12	27	2	2.7

3. Penalization of the centered fluxes by dissipative terms

For complex problems as usually encountered in industry, the meshes are built by using specific tools which, generally, do not generate automatic regular meshes. In particular, important differences between the sizes of the biggest and the smallest cells can be observed, as well as very distorted cells. In such cases, two problems appear:

- The use of a centered fluxes formulation can sometimes generate numerical spurious modes which degrade the accuracy of the solution.
- If strong cell-size disparities are encountered, it becomes necessary to use a small global time step which results in an important loss of efficiency of the scheme. In such cases, the advantages (accuracy and memory) of the DG method have a prohibitive cost: the computational time.

The second point will be treated in the next section by introducing local time-stepping strategies. For the first point, several studies [20,21] have been done to analyze the importance of the dispersive errors and spurious modes in DG schemes. The solution proposed here to reduce or eliminate spurious mode consists in adding some dissipative terms in the numerical scheme. Indeed, in the formalism (3) equivalent to the Maxwell equations, jump terms have been added on $E \times n$ and $H \times n$, and dissipative jump terms on $n \times (E \times n)$ and $n \times (H \times n)$. In the previous scheme we neglected the dissipative terms. A numerical study highlights their importance in the method when the meshes are very distorted [9]. In particular their ability to reduce considerably the spurious modes have to be mentioned. Then, we introduce these dissipative terms through penalization terms with two positive coefficients λ_{PE}, λ_{PH} without modifying the time approximation. The new formulation of the problem on each element K becomes:

$$\begin{cases} \int_K \varepsilon \partial_t E_h \cdot \psi \,\mathrm{d}x + \int_K \sigma E_h \cdot \psi \,\mathrm{d}x \\ \quad = \int_K \nabla \times H_h \cdot \psi \,\mathrm{d}x + \int_{\partial K} \left(\beta^K_{\partial K} (\llbracket H_h \times n_K \rrbracket^K_{\partial K} + \mathrm{sign}(\beta^K_{\partial K}) \lambda_{PE} \llbracket n_K \times (E_h \times n_K) \rrbracket^K_{\partial K}) \right) \cdot \psi \,\mathrm{d}s, \\ \int_K \mu \partial_t H_h \cdot \phi \,\mathrm{d}x = -\int_K \nabla \times E_h \cdot \phi \,\mathrm{d}x + \int_{\partial K} \left(\gamma^K_{\partial K} (\llbracket E_h \times n_K \rrbracket^K_{\partial K} + \mathrm{sign}(\gamma^K_{\partial K}) \lambda_{PH} \llbracket n_K \times (H_h \times n_K) \rrbracket^K_{\partial K}) \right) \cdot \phi \,\mathrm{d}s. \end{cases}$$

In this expression, the dissipative terms of the forms $\int_{\partial K} [n_K \times (v \times n_K)] \cdot \phi \,\mathrm{d}s$ can be evaluated as follows:

$$\int_{\partial K} \llbracket n_K \times (v \times n_K) \rrbracket \cdot \Phi \,\mathrm{d}s = \int_{\partial K} n_K \times (v_{K'} \times n_K) \cdot \phi \,\mathrm{d}s - \int_{\partial K} n_K \times (v_K \times n_K) \cdot \phi \,\mathrm{d}s, \tag{6}$$

where v_K and $v_{K'}$ are the fields taken respectively to the cells K and K', adjacent at the face ∂K. We obtain for the term with v_K :

$$\begin{aligned} \int_{\partial K} n_K \times (v_K \times n_K) \cdot \phi \,\mathrm{d}s &= \int_{\partial K} (v_K \times n_K) \cdot (\phi \times n_K) \,\mathrm{d}s \\ &= \int_{\widehat{\partial K}} \frac{DF_K}{J_K \| DF_K^{*-1} \hat{n}_K \|} (\hat{v}_K \times \hat{n}_K) \cdot \frac{DF_K}{J_K \| DF_K^{*-1} \hat{n}_K \|} (\hat{\phi} \times \hat{n}_K) |J_K| \| DF_K^{*-1} \hat{n}_K \| \mathrm{d}\hat{s} \\ &= \int_{\widehat{\partial K}} \frac{1}{|J_K| \| DF_K^{*-1} \hat{n}_K \|} DF_K^* DF_K (\hat{v} \times \hat{n}_K) \cdot (\hat{\phi} \times \hat{n}_K) \mathrm{d}\hat{s} \end{aligned}$$

and for the term with $v_{K'}$:

$$\begin{aligned} \int_{\partial K} n_K \times (v_{K\prime} \times n_K) \cdot \phi \,\mathrm{d}s &= \int_{\partial K} (v_{K\prime} \times n_K) \cdot (\phi \times n_K) \,\mathrm{d}s \\ &= \int_{\widehat{\partial K}} (v_{K'} \circ F_K(\hat{x}) \times n_K) \cdot \frac{DF_K}{J_K \| DF_K^{*-1} \hat{n} \|} (\hat{\phi} \times \hat{n}) |J_K| \| DF_K^{*-1} \hat{n} \| \mathrm{d}\hat{s}. \end{aligned}$$

The maps $F_{K'}$ and F_K give $F_{K'}(\partial \hat{K}') = \partial K = F_K(\partial \widehat{K})$. Consider the change of variable from $\partial \widehat{K}$ to $\partial \hat{K}'$, by using $S_{K'K} = F_K^{-1} \circ F_{K'}$ on the previous integral, we obtain:

$$-\int_{\widehat{\partial K'}} \frac{DF_{K'}}{J_{K'} \left\| DF_{K'}^{*-1} \times \hat{n}_{K'} \right\|} (\hat{v}_{K'} \times \hat{n}_{K'}) \cdot \frac{DF_K \circ S_{K'K}}{(J_K \| DF_K^{*-1} \hat{n}_K \|) \circ S_{K'K}} (\hat{\phi} \times \hat{n}_K) \circ S_{K'K} (|J_K| \| DF_K^{*-1} \hat{n}_K \|) \circ S_{K'K} \,\mathrm{d}\hat{s}',$$

where $n_{K'} = -n_K$. By using:

$$J_{K'}\|DF_{K'}^{*-1} \times \hat{n}_{K'}\| = (J_K\|DF_K^{*-1} \times \hat{n}_K\|) \circ S_{K'K},$$

we finally obtain:

$$-\int_{\widehat{\partial K'}} \frac{DF_{K'}^{*}(DF_K \circ S_{K'K})}{|J_{K'}|\|DF_{K'}^{*-1} \times \hat{n}_{K'}\|}(\hat{v}_{K'} \times \hat{n}_{K'}) \cdot (\hat{\phi} \times \hat{n}_K) \circ S_{K'K}\, \mathrm{d}\hat{s}'.$$

On the new expression of the jump integrals, we need to evaluate and store a 3×3 matrix $DF_K^* DF_K$ at each unknown of each surface of the cell K. Although this modification induces an increase of memory storage, the method remains advantageous because the others integrals in the formulation are not modified and need low memory storage.

3.1. L^2-Stability of the spatial dissipative scheme

In [8] a stability result has been given for our spatial non-dissipative DG method. When dissipative terms are added, it is important to obtain a stable numerical method. In this subsection, we propose a condition to ensure the stability of our spatial dissipative DG method.

Recall the dissipative DG method:

$$\begin{cases} \int_K \varepsilon_K \frac{E_h^{n+1}-E_h^n}{\Delta t} \cdot \psi\, \mathrm{d}x = \int_K \nabla \times H_h^{n+\frac{1}{2}} \cdot \psi\, \mathrm{d}x + \int_{\partial K} \left(\beta [\![H_h^{n+\frac{1}{2}} \times n_K]\!]_{\partial K}^K + \frac{\lambda}{Z_{\partial K}} [\![n_K \times (E_h^n \times n_K)]\!]_{\partial K}^K\right) \cdot \psi\, \mathrm{d}s, \\ \int_K \mu_K \frac{H_h^{n+\frac{1}{2}}-H_h^{n-\frac{1}{2}}}{\Delta t} \cdot \phi\, \mathrm{d}x = -\int_K \nabla \times E_h^n \cdot \phi\, \mathrm{d}x + \int_{\partial K} \left(\gamma [\![E_h^n \times n_K]\!]_{\partial K}^K + \frac{\lambda}{Y_{\partial K}} [\![n_K \times \left(H_h^{n-\frac{1}{2}} \times n_K\right)]\!]_{\partial K}^K\right) \cdot \phi\, \mathrm{d}s, \end{cases} \tag{7}$$

where $Z_\Gamma = \frac{1}{2}\left(\sqrt{\frac{\mu_K}{\varepsilon_K}} + \sqrt{\frac{\mu_{K'}}{\varepsilon_{K'}}}\right)$ and $Y_\Gamma = \frac{1}{2}\left(\sqrt{\frac{\varepsilon_K}{\mu_K}} + \sqrt{\frac{\varepsilon_{K'}}{\mu_{K'}}}\right)$ with $\Gamma = K \cap K\prime$ and considering $\lambda_{PE} = \frac{\lambda}{Z_{\partial K}}$, $\lambda_{PH} = \frac{\lambda}{Y_{\partial K}}$.

To generalize the L^2 stability property, we take also a permittivity ε_k and a permeability μ_K constant by cell.

Taking up the L^2-stability analysis carried out in [8], we easily obtain:

Proposition 1.

$$\mathcal{E}_h^{n+1} - \mathcal{E}_h^n = -\lambda \Delta t \sum_{\Gamma \in \mathcal{F}^i} \int_\Gamma \left(\frac{1}{Z_\Gamma}[\![E_h^n \times n_\Gamma]\!] \cdot [\![E_h^n \times n_\Gamma]\!] + \frac{1}{Z_\Gamma}[\![E_h^n \times n_\Gamma]\!] \cdot [\![E_h^{n+1} \times n_\Gamma]\!] + \frac{1}{Y_\Gamma}[\![H_h^{n+\frac{1}{2}} \times n_\Gamma]\!] \cdot [\![H_h^{n+\frac{1}{2}} \times n_\Gamma]\!] + \frac{1}{Y_\Gamma}[\![H_h^{n-\frac{1}{2}} \times n_\Gamma]\!] \cdot [\![H_h^{n+\frac{1}{2}} \times n_\Gamma]\!]\right),$$

where $\mathcal{E}_h^n = \sum_{K \in \mathcal{T}_h}(\int_K \varepsilon_K E_{h,K}^n \cdot E_{h,K}^n\, \mathrm{d}x + \int_K \mu_K H_{h,K}^{n+\frac{1}{2}} \cdot H_{h,K}^{n-\frac{1}{2}}\, \mathrm{d}x)$ *and* $\mathcal{F}^i$ *is the set of internal faces of the mesh* $\mathcal{T}$ *i.e. if* $\Gamma \in \mathcal{F}^i$ *then* $\exists K, K' \in \mathcal{T}_h$ *such that* $\Gamma = K \cap K'$.

Proof. This proof is classical and does not raise any difficulty. That is why, we only give its sketch.

In order to derive this result, we take the test functions

$$\psi = E_h^{n+1} + E_h^n \quad \text{and} \quad \phi = H_h^{n+\frac{1}{2}}$$

Next, we test the first equation of (7) at time n and the second at times n and $n+1$. Finally, by adding these three equations for all cells of the mesh $\mathcal{T}$, we obtain the result.

In the case where the scheme is not dissipative (i.e. $\lambda = 0$) we obviously find the well-known discrete energy conservation i.e. $\mathcal{E}_h^{n+1} = \mathcal{E}_h^n$. □

The estimate $ab \leqslant (a^2 + b^2)/2$ leads to:

$$\mathcal{E}_h^{n+1} - \mathcal{E}_h^n \leqslant \frac{\lambda \Delta t}{2} \sum_{\Gamma \in \mathcal{F}^i} \left(-\frac{1}{Z_\Gamma}\|[\![E_h^n \times n_\Gamma]\!]\|_{0,\Gamma}^2 + \frac{1}{Z_\Gamma}\|[\![E_h^{n+1} \times n_\Gamma]\!]\|_{0,\Gamma}^2 - \frac{1}{Y_\Gamma}\|[\![H_h^{n+\frac{1}{2}} \times n_\Gamma]\!]\|_{0,\Gamma}^2 + \frac{1}{Y_\Gamma}\|[\![H_h^{n-\frac{1}{2}} \times n_\Gamma]\!]\|_{0,\Gamma}^2\right), \tag{8}$$

where $\|\cdot\|_{0,X}$ is the L^2 norm on X.

So, one can define a better adapted discrete energy:

$$\widetilde{\mathcal{E}}_h^n = \mathcal{E}_h^n - \frac{\lambda\Delta t}{2}\|[\![E_h^n \times n_\Gamma]\!]\|^2_{0,\mathcal{F}^i,Z} - \|[\![H_h^{n-\frac{1}{2}} \times n_\Gamma]\!]\|^2_{0,\mathcal{F}^i,Y}$$

with $\|\cdot\|^2_{0,\mathcal{F}^i,X} = \sum_{\Gamma\in\mathcal{F}^i}\frac{1}{X_\Gamma}\|\cdot\|^2_{0,\Gamma}$. The estimate (8) becomes:

$$\widetilde{\mathcal{E}}_h^{n+1} - \widetilde{\mathcal{E}}_h^n \leqslant 0.$$

To prove the L^2-stability of the scheme, one must find a CFL condition for which $\widetilde{\mathcal{E}}_h^n$ is a positive definite quadratic form [8].

Noting that

$$\widetilde{\mathcal{E}}_h^n \geqslant \mathcal{E}_h^n - \frac{\lambda\Delta t}{2}\|[\![E_h^n \times n_\Gamma]\!]\|^2_{0,\mathcal{F}^i,Z}$$

and that

$$\begin{aligned}
\|[\![E_h^n \times n_\Gamma]\!]\|^2_{0,\mathcal{F}^i,Z} &= \sum_{\Gamma=K\cap K'\in\mathcal{F}^i} \frac{2}{\sqrt{\frac{\mu_K}{\varepsilon_K}} + \sqrt{\frac{\mu_{K'}}{\varepsilon_{K'}}}}\|[\![E_h^n \times n_\Gamma]\!]\|^2_{0,\Gamma} \\
&\leqslant \sum_{\Gamma=K\cap K'\in\mathcal{F}^i} \frac{4}{\sqrt{\frac{\mu_K}{\varepsilon_K}} + \sqrt{\frac{\mu_{K'}}{\varepsilon_{K'}}}}(\|E_{h,K}^n \times n_\Gamma\|^2_{0,\Gamma} + \|E_{h,K'}^n \times n_\Gamma\|^2_{0,\Gamma}) \\
&\leqslant 4\sum_{\Gamma=K\cap K'\in\mathcal{F}^i}\left(\frac{c_K}{1+\sqrt{\frac{\varepsilon_K\mu_{K'}}{\varepsilon_{K'}\mu_K}}}\|E_{h,K}^n \times n_\Gamma\|^2_{0,\Gamma} + \frac{c_{K'}}{1+\sqrt{\frac{\varepsilon_{K'}\mu_K}{\varepsilon_K\mu_{K'}}}}\|E_{h,K'}^n \times n_\Gamma\|^2_{0,\Gamma}\right) \\
&\leqslant 4\sum_{K\in\mathcal{T}_h} c_K\|\widetilde{E}_{h,K}^n \times n_K\|^2_{0,\partial K^i} \quad (\partial K^i = \text{the set of faces of } K \text{ belonging to } \mathcal{F}^i) \\
&\leqslant 4\lambda_{\max}\,(\widehat{\mathcal{D}}^{-\frac{1}{2}}\widehat{\mathcal{B}}\widehat{\mathcal{D}}^{-\frac{1}{2}})\sum_{K\in\mathcal{T}_h} c_K\|\widehat{E}_K\|^2_{0,\widehat{K}} \text{ see [8]},
\end{aligned}$$

where $\lambda_{\max}(A)$ corresponds to the greatest eigenvalue of the matrix A, $c_K = 1/\sqrt{\varepsilon_K\mu_K}$, $\widetilde{E}_{h,K}^n = E_{h,K}^n\sqrt{\varepsilon_K}$ and $\widehat{\mathcal{D}}$, $\widehat{\mathcal{B}}$ are the $3(r+1)^3 \times 3(r+1)^3$ matrices defined by: $\forall l,\ l' \in \{1,2,3\}$ and $\forall I = (i,j,k),\ I' = (i',j',k') \in \{1,\ldots,r+1\}^3$

$$\widehat{\mathcal{D}}((l,I),(l',I')) = \delta_{ll'}\delta_{II'}\omega_{ijk}$$

$$\widehat{\mathcal{B}}((l,I),(l',I')) = \int_{\partial\widehat{K}}(\hat{\varphi}_{ijk}^l \times \hat{n})\cdot(\hat{\varphi}_{i'j'k'}^{l'} \times \hat{n})\mathrm{d}\hat{s},$$

it is easy to see that the stability condition in [8] becomes:

$$\frac{\Delta t}{\Lambda_K} < \frac{2}{c_K}\frac{1}{\sqrt{\lambda_{\max}(\widehat{\mathcal{D}}^{-\frac{1}{2}}\widehat{\mathcal{R}}\widehat{\mathcal{D}}^{-\frac{1}{2}})} + \left(\frac{1}{2}\max_{1\leqslant i\leqslant nbfi_K}\left(\sqrt{\frac{\mu_K}{\mu_{V(i,K)}}},\sqrt{\frac{\varepsilon_K}{\varepsilon_{V(i,K)}}}\right) + 4\lambda\right)\lambda_{\max}(\widehat{\mathcal{D}}^{-\frac{1}{2}}\widehat{\mathcal{B}}\widehat{\mathcal{D}}^{-\frac{1}{2}})},$$

where $\Lambda_K = \min_{1\leqslant i,j,k\leqslant r+1}\left(\frac{|J_K(\hat{\mathbf{x}}_{ijk})|}{\lambda_{\max}((DF_K^*DF_K)(\hat{\mathbf{x}}_{ijk}))}\right)$ (in the case of a uniform Cartesian grid whose the spatial step is h, $\Lambda_K = h$).

So, the dissipative DG method using a leap-frog approximation in time is L^2-stable. As we have noted in practice, we can see that this condition is slightly more restrictive than the one obtained with the non-dissipative scheme. This is due to the backward discretization for the time approximation of penalization terms.

3.2. A priori error estimate

The advantage of the proposed spatial dissipative scheme is significant with strongly distorted meshes. Particularly, by a mathematical analysis we can demonstrate a gain in the order of convergence of the scheme which implies the convergence for all spatial orders of approximation.

In [10], a complete error analysis of the non-dissipative scheme has been carried out. In particular, we have pointed out that the choice of the approximation (hexahedrals, centered flux and the presence of the Jacobian matrix in $\mathbf{V}_r$) can imply a loss of spatial convergence and the Q_1 scheme can even become no-convergent. By adding the penalization terms, a similar study can be made on the convergence of the dissipative scheme.

Let (E,H) and (E_h,H_h) be, respectively, the exact solution of the Maxwell equations and the approximate DG solution belonging to V_r. Then, to evaluate a convergence of the DG method, we evaluate an overestimation of $\|(E-E_h,H-H_h)\|_*$ by a term depending of the spatial step size and the order of the DG scheme. The $\|(\cdot,\cdot)\|_*$ is the energy norm defined by $\|(E,H)\|_*^2=\int_\Omega(\varepsilon E\cdot E+\mu H\cdot H)\mathrm{d}x=\|E\|_{0,\epsilon,\Omega}^2+\|H\|_{0,\mu,\Omega}^2$, where $\|E\|_{0,\epsilon,\Omega}^2=\int_\Omega(\varepsilon E\cdot E)\mathrm{d}x$ and $\|H\|_{0,\mu,\Omega}^2=\int_\Omega(\mu H\cdot H)\mathrm{d}x$.

Consider $(u,w)\in V_r\times V_r$, we write $E-E_h=E-v+v-E_h=\Delta_E^P-\Delta_E^I$ and $H-H_h=H-w+w-H_h=\Delta_H^P-\Delta_H^I$ with $\Delta_E^P=E-v$, $\Delta_E^I=E_h-v$, $\Delta_H^P=H-w$ and $\Delta_H^I=H_h-w$.We have the two following propositions:

Proposition 2. *Let $(v,w)\in\mathbf{V}_r\times\mathbf{V}_r$ be the solution of the problem: $\forall(v',w')\in\mathbf{V}_r\times\mathbf{V}_r$ and $\forall K\in\mathcal{T}$,*

$$\begin{aligned}&\int_K\varepsilon v\cdot v'\,\mathrm{d}x+\int_K\nabla\times w\cdot v'\,\mathrm{d}x-\int_{\partial K}(\beta[\![w\times n]\!]_{\partial K}^K+\lambda[\![n\times(v\times n)]\!]_{\partial K}^K)\cdot v'\,\mathrm{d}s=l_1(v'),\\&\int_K\mu w\cdot w'\,\mathrm{d}x-\int_K\nabla\times v\cdot w'\,\mathrm{d}x-\int_{\partial K}(\gamma[\![v\times n]\!]_{\partial K}^K+\lambda[\![n\times(w\times n)]\!]_{\partial K}^K)\cdot w'\,\mathrm{d}s=l_2(w'),\end{aligned}\tag{9}$$

where l_1, l_2 are the two linear forms on $\mathbf{V}_r$ defined by:

$$\begin{aligned}l_1(v')&=\int_K\varepsilon E\cdot v'\,\mathrm{d}x+\int_K\nabla\times H\cdot v'\,\mathrm{d}x,\\l_2(w')&=\int_K\mu H\cdot w'\,\mathrm{d}x-\int_K\nabla\times E\cdot w'\,\mathrm{d}x.\end{aligned}$$

Then, we have:

$$\frac{\mathrm{d}}{\mathrm{d}t}\|(\Delta_E^I,\Delta_H^I)\|_*\leqslant\|\Delta^P_{\frac{\partial E}{\partial t}}\|_{0,\varepsilon,\Omega}+\|\Delta^P_{\frac{\partial H}{\partial t}}\|_{0,\mu,\Omega}+\|\Delta_E^P\|_{0,\varepsilon,\Omega}+\|\Delta_H^P\|_{0,\mu,\Omega}.\tag{10}$$

Proposition 3. *If we assume that the exact solution verifies $(E,H)\in H^{s+1}(\mathcal{T})$ for $s\geqslant 0$, then there exists a constant $C>0$ such that*

$$\|(\Delta_E^P,\Delta_H^P)\|_*\leqslant Ch^{min(s-\frac{1}{2},r-\frac{1}{2})}max(\|E\|_{s+1,h},\|H\|_{s+1,h}),$$

where $H^s(\mathcal{T})=\{v\in[L^2(\Omega)]^3:\forall K\in\mathcal{T},\ v_{|K}\in[H^s(K)]^3\}$ and $\|v\|_{s,h}^2=\sum_{K\in\mathcal{T}}\|v\|_{s,K}^2$.

The technical proofs of these two propositions are given at the Appendix A.

By using Propositions 2 and 3 and the Gronwall lemma on the time interval $(0,T)$, we have:

Theorem 1. *Let r be a positive integer. Assume that the exact solution verifies $(E,H)\in H^{s+1}(\mathcal{T})$ and $(\frac{\partial E}{\partial t},\frac{\partial H}{\partial t})\in H^{s'+1}(\mathcal{T})$ for $s,s'\geqslant 0$ real and $0<h_K\leqslant 1$. Then, we have the global estimate of the interpolation error:*

$$\|(\Delta_E^I,\Delta_H^I)\|_*(T)\leqslant\|(\Delta_E^I,\Delta_H^I)\|_*(0)+CTh^{min(s-\frac{1}{2},s'-\frac{1}{2},r-\frac{1}{2})}A(T,E,H),\tag{11}$$

where

$$A(T,E,H)=\max_{t\in(0,T)}\left(\|E\|_{s+1,h}(t),\|H\|_{s+1,h}(t),\left\|\frac{\partial E}{\partial t}\right\|_{s'+1,h}(t),\left\|\frac{\partial H}{\partial t}\right\|_{s'+1,h}(t)\right).$$

Finally, by using (11) and (3), we deduce the error of the DG-scheme by:

$$\|(E-E_h, H-H_h)\|_*^2 \leqslant 2(\|(\Delta_E^P, \Delta_H^P)\|_*^2 + \|(\Delta_E^I, \Delta_H^I)\|_*^2).$$

In conclusion, if the exact solution is smooth enough, the convergence rate for the penalized scheme is $r-\frac{1}{2}$ versus $r-1$ for the non-dissipative scheme. So, the dissipative terms ensure the L^2-convergence for the Q_1 approximation.

3.3. Some numerical results

In [10], we have proved that the value $r-1$ for the spatial convergence rate (in L^2 norm) of non-dissipative scheme seems to be optimal for the general unstructured meshes. The previous error analysis shows that this bound becomes $r-1/2$ when one adds dissipative terms. These two results are sufficient to affirm that the dissipative scheme is better convergent than the non-dissipative one. In this part, we just illustrate this result by some numerical results.

To underline the convergence results for the Q_1 approximation, we give two examples comparing the dissipative and the non-dissipative approaches. The first example is the previous cavity problem treated in Section 2. For several non-regular unstructured meshes of the cavity with an assimilate decreasing spatial step size h, we compare in Table 2 the errors in norm L^2 between the analytic solution and the solutions obtained with the dissipative and the non-dissipative Q_1 spatial approximation.

We can see in this table a better convergence of the scheme by considering dissipative terms than without these terms. Moreover, the spatial rate of convergence tends to the theoretical one i.e. $0(h^0)$ and $0(h^{0.5})$ when h tends to zero. Fig. 2 shows also comparison on accuracy between the solutions obtained with the two schemes for a same mesh configuration and for an integration time equivalent to 10 wavelengths. We note in this figure, on the first curves, the advantage of the dissipative approach. This advantage is clearly due, as pointed out in the second curves of the figure, to the dispersive error induced by the non-dissipative scheme. Indeed, we can show by a mathematical study in one dimension that the dissipative scheme is less dispersive than the non-dissipative scheme (order 4 instead of order 2 [13,8]).

This cavity example shows the advantages to take into account the dissipative terms in our formalism when the mesh is non-regular, but for this kind of problem, a Q_1 approximation is not the best choice and an approximation of higher order will be more appropriate in order to decrease dissipative and dispersive errors. In particular, this is indicated to observe on long time integration.

However, for scattering problems, the Q_1 approximation can sometimes be sufficient to obtain accurate solution and taking into account the dissipative terms improves the efficiency of the method. The second example proposed in this section gives an application related to this kind of problems. The problem consists in evaluating at a given test-point the electromagnetic fields scattered by a perfectly metallic sphere (center $=(0,0,0)$ and radius $=0.5$ m) illuminated with an incident plane wave given by $E_y(t,x,y,z) = 377\exp\left(-\left(\frac{t+\frac{z-1}{3e8}-1e-8}{5e-9}\right)^2\right)$. In Fig. 3, we compare the results obtained by using or not the dissipative terms in the scheme. We can see different solutions obtained with the non-dissipative Q_1 and Q_2 approximations, the dissipative Q_1 approximation and the FDTD method, being assumed here as the reference solution. The FDTD solution has been obtained for a mesh where the cell size is less than the smallest wavelength of the source spectrum divided by 80. This solution is quasi-similar for meshes with smaller cell sizes. We

Table 2
Error between numerical and analytical solutions for different spatial steps

Method	Without dissipative terms		With dissipative terms	
	L^2 error	Order	L^2 error	Order
h	0.01478	×	0.0108	×
$h1=h/2$	0.0122	0.27	0.0073	0.565
$h2=h1/1.5$	0.0115	0.13	0.0057	0.55

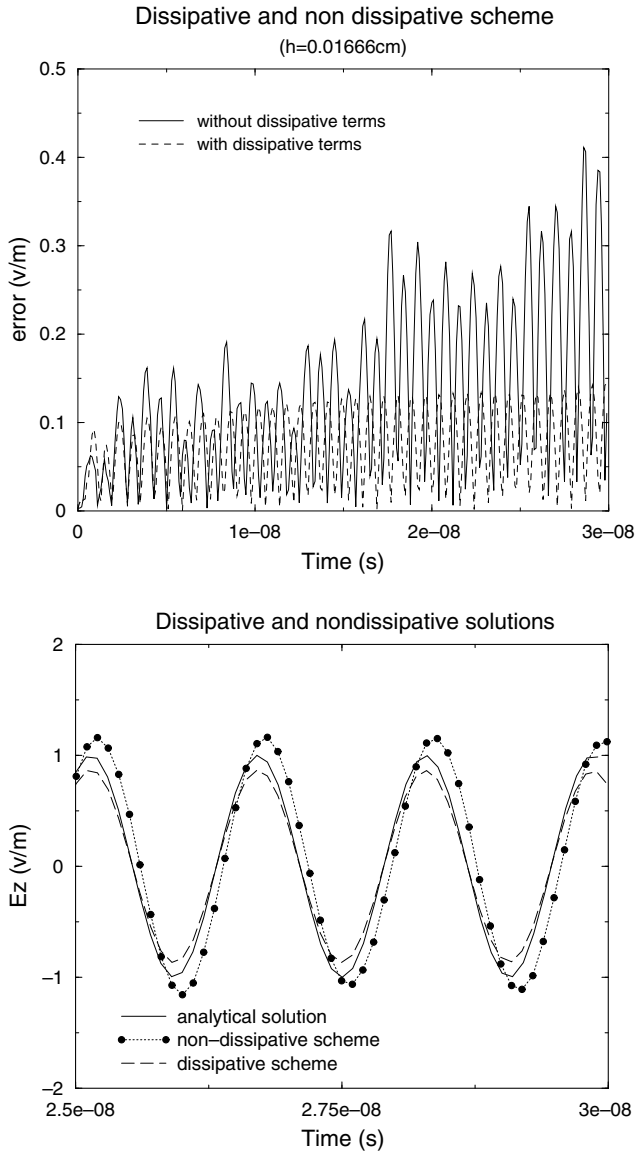

Fig. 2. Comparison between non-dissipative and dissipative schemes.

can notice that the solution obtained with the non-dissipative Q_1 approximation has a strange behavior. The use of a Q_2 approximation in the non-dissipative scheme improves the solution. However, this solution remains less accurate than the solution obtained with the dissipative Q_1 approximation. Indeed, little oscillations appears in the Q_2-approximation solution due certainly to spurious modes. In fact, for scattering problems, the advantage of using dissipative terms in our DG scheme on non-regular meshes is double: We obtain more accurate solutions with low spatial order approximation and we require less computational time.

4. Local time-stepping strategy based upon a leap-frog time scheme

The DG scheme we presented is based on an explicit leap-frog time discretization, which is a well-know scheme in the electromagnetism community [2,15]. Nevertheless, when dealing with unstructured meshes, there can be strong cell size disparities and, to ensure stability, the global time step is constrained by the smallest cell

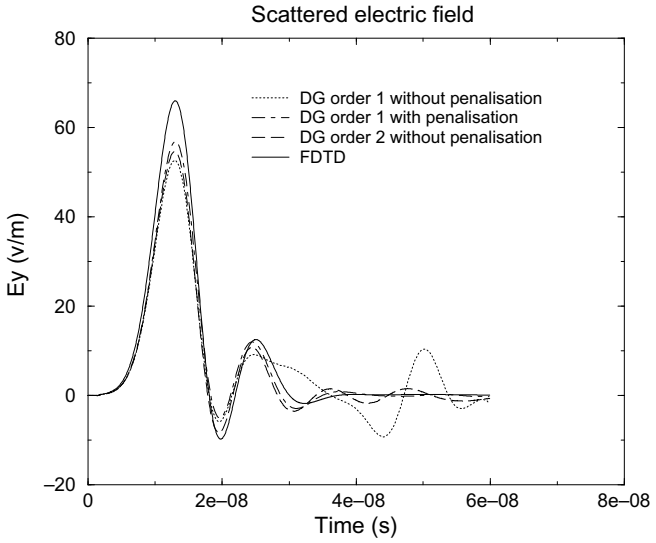

Fig. 3. Electric fields located at a given test-point $A = (1, 0, 0)$.

of the mesh; this implies an important increase of computational time. To avoid this problem, a solution could be to take an implicit scheme for time discretization, but this solution implies to solve a big linear system at each time step. In this approach, direct solvers cannot be used because they need to store a too big matrix. In other way, the possibility to obtain fast and convergent iterative method to solve this kind of problem, stays, at our knowledge, a difficult and not solved challenge. Consequently, we choose another solution which consists to introduce a local time-stepping strategy in our explicit scheme. Indeed, the time step imposed by the smallest cell is not necessary for all cells to ensure the stability of the scheme in the computational domain. In the literature, for Maxwell's equations, we can find local time-stepping methods which ensure or not a condition of stability. In particular, a method based on a FDTD scheme has been proposed in [14] to ensure an energy conservation. But, for 3D-Maxwell's equations, this method leads to a numerical scheme too expensive in terms of memory and computational time. Consequently, local time-stepping strategies based upon interpolations and fully explicit schemes, where a stability condition is difficult to be proved, remain the most attractive. In this paper, we focus our investigations on a method of this last family to improve our DG method.

4.1. 2-class and multi-class methods

Starting from our DG scheme with leap-frog time discretization, we proposed in [8] a 2-classes method using interpolations. In this approach, the computational domain is split into two parts: the first one composed of cells evaluated with a time step adapted to the smallest cells of the mesh, and the second one on which cells are evaluated with a larger time step. The largest time step is taken as a multiple of the smallest one in order to ensure coincidence at each step of the process, and interpolations are used to approximate unknown fields. This method gives good results and the computational time is considerably reduced with meshes composed of small and big cells. However, in general, the range of cells size have a continuous progression from smallest to biggest ones and, in the case of strongly refined unstructured meshes, it is widely required to use more than two classes of cells to reduce the CPU time cost of simulations. Unfortunately, using interpolations with more than two classes is too expensive in term of computational time and multi-class strategies must be investigated.

In this kind of multi-class methods, a non-dissipative DG approach, proposed by Piperno [15], was presented as symplectic [16], and therefore was supposed to conserve an energy quantity. It is based on the Verlet scheme, which is a reorganization of the classical leap-frog scheme into three steps. Let E^n and H^n be the

electric and magnetic fields at the time step n, the values of the fields E^{n+1} and H^{n+1} at the time $n+1$ by using the Verlet scheme are given by:

$$\begin{cases} H^{n+\frac{1}{2}} = H^n - \frac{\Delta t}{2} M_\mu^{-1} S E^n, \\ E^{n+1} = E^n + \Delta t M_\varepsilon^{-1} S H^{n+\frac{1}{2}}, \\ H^{n+1} = H^{n+\frac{1}{2}} - \frac{\Delta t}{2} M_\mu^{-1} S E^{n+1}, \end{cases} \tag{12}$$

where Δt, M_ε, M_μ and S are, respectively, the time step, the mass matrices for electric and magnetic equation and the matrix related to the curl operator.

In his multi-class approach, Piperno bulks the cells into N sets or classes $1, 2, \ldots, N-1, N$ which are associated to the respective time-steps $\frac{\Delta t}{2^{N-1}}, \frac{\Delta t}{2^{N-2}}, \ldots, \frac{\Delta t}{2}, \Delta t$. Then, the smallest cells are in class 1 and the largest cells in class N. In the process, for an evaluation of the fields at a step Δt, the number of field evaluations inside each class is different. In Fig. 4 the steps are labeled in the order in which they are executed in the process.

In the Fig. 4, we can notice also that the multi-class approach can be defined at each time step Δt by a recursive process labeled $R^N(\Delta t)$ and given by:

$$\begin{cases} \text{Evaluate } R^{N-1}\left(\frac{\Delta t}{2}\right), \\ \text{Evaluate the cells into class } N \text{ by using Eq. (12)}, \\ \text{Evaluate } R^{N-1}\left(\frac{\Delta t}{2}\right) \end{cases} \tag{13}$$

with the convention that R^0 performs no operation.

Note that this time domain scheme consists in a recursive call of the Verlet scheme on different classes (for $N = 1$, we retrieve the original Verlet scheme). However, even if the Verlet scheme is symplectic, we can not a priori affirm that this recursive scheme is symplectic too. Indeed, calling the Verlet scheme on different classes requires values of the fields at some unknown times. To palliate this difficulty, the last known fields available are used. Consequently, the scheme which is recursively called in (13) is not exactly the Verlet one, and the symplectic and stability properties of this multi-classes method are still an open question, even if an energy conservation is proved in [15] for $N = 2$. In particular, for long time simulations, it can be necessary to reduce the time steps in order to avoid instabilities. Nevertheless, this recursive scheme remains attractive and it can be easily adapted to a dissipative scheme with the same advantages as for non-dissipative scheme. Indeed,

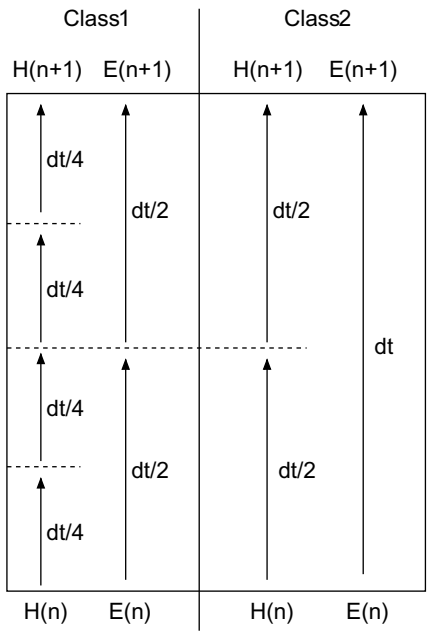

Fig. 4. Operations in a time step of the Piperno scheme with two classes.

regardless of the number of classes N, this scheme is easy to implement, fully explicit, it does not need any additional storage and gives good results: the numerical solution is comparable to standard ones and the computation time is significantly reduced.

From the same idea, we present here a leap-frog based recursive method, better adapted to our scheme and more efficient in terms of computational time.

4.2. Recursive leap-frog method

To make comparison with the Piperno method, we describe the recursive leap-frog method in the case of a spatial non-dissipative formulation. To take into account a spatial dissipative formulation, we only need to add new jump terms which are split like the non-dissipative jump terms. This does not induce any particular difficulty and the analysis done in this section on comparison between the different methods remains the same. Indeed, for dissipative or non-dissipative formulation, the number of classes defined depends on the shape of the cell and of the variation of the time step in the set of cells. This last quantity is approximately the same for the two formulations.

For practical reasons, we rewrite our Discontinuous Galerkin formulations defined by Eq. (5) under the equivalent form [15]:

$$\begin{cases} M_\varepsilon \partial_t E + M_\sigma E = A_H H - S^{i-} H = SH, \\ M_\mu \partial_t H = -A_E E + S^{i-} E = -S^T E, \end{cases} \tag{14}$$

by splitting in (5), the jump terms S^i and $(S^i)^T$ in a cell into two parts:

- part inside the cell itself: S^{i+} and $(S^{i+})^T$,
- part outside the cell S^{i-} and $(S^{i-})^T$.

Then we obtain $A_E = R + S^{i+}$ and $A_H = R - (S^{i+})^T - S^b$. For the following, we consider $M_\sigma = 0$ to simplify the expressions but there is no difficulty to take into account this term on the recursive leap-frog method. As for the previous scheme, the cells of the mesh are grouped into N integration classes i, associated to the time step $(2m+1)^{N-i}\Delta t_{\min}$, where m is a strictly positive integer and $\Delta t_{\min}$ the time step corresponding to the smallest cell of the mesh. In the sequel, we consider the case $m = 1$, which means that there is a factor 3 between the time steps of consecutive classes.

We recall hereafter the expression of the leap-frog scheme with a time-step Δt at the step n is given by:

$$\begin{cases} M_\mu \frac{H^{n+1/2} - H^{n-1/2}}{\Delta t} = -S^T E^n, \\ M_\varepsilon \frac{E^{n+1} - E^{n-1}}{\Delta t} = SH^{n+1/2}. \end{cases} \tag{15}$$

For $N = 2$, by considering (14), we propose the following multi-class leap-frog method at cells located at the interface between class 1 and 2 can be written:

$$\begin{cases} M_2^\mu \frac{H_2^{n+\frac{1}{2}} - H_2^{n-\frac{1}{2}}}{\Delta t} = -A_2 E_2^n + S_{21}^T E_1^n, \\ M_1^\mu \frac{H_1^{n+\frac{1}{6}} - H_1^{n-\frac{1}{6}}}{\Delta t/3} = -A_1 E_1^n + S_{12}^T E_2^n, \\ M_1^\varepsilon \frac{E_1^{n+\frac{2}{6}} - E_1^n}{\Delta t/3} = A_1 H_1^{n+\frac{1}{6}} - S_{12} H_2^{n+\frac{1}{2}^*}, \\ M_1^\mu \frac{H_1^{n+\frac{1}{2}} - H_1^{n+\frac{1}{6}}}{\Delta t/3} = -A_1 E_1^{n+\frac{2}{6}} + S_{12}^T E_2^{n^*}, \\ M_2^\varepsilon \frac{E_2^{n+1} - E_2^n}{\Delta t} = A_2 H_2^{n+\frac{1}{2}} - S_{21} H_1^{n+\frac{1}{2}}, \\ M_1^\varepsilon \frac{E_1^{n+\frac{4}{6}} - E_1^{n+\frac{2}{6}}}{\Delta t/3} = A_1 H_1^{n+\frac{1}{2}} - S_{12} H_2^{n+\frac{1}{2}}, \\ M_1^\mu \frac{H_1^{n+\frac{5}{6}} - H_1^{n-\frac{1}{2}}}{\Delta t/3} = -A_1 E_1^{n+\frac{4}{6}} + S_{12}^T E_2^{n+1^*}, \\ M_1^\varepsilon \frac{E_1^{n+1} - E_1^{n+\frac{4}{6}}}{\Delta t/3} = A_1 H_1^{n+\frac{5}{6}} - S_{12} H_2^{n+\frac{1}{2}^*}, \end{cases} \tag{16}$$

where in the matrices, the subscripts 1, 2, 21 and 12 are identified, respectively, to cells in class 1, 2 and terms in jumps coming from cells located in class 1 (respectively, 2) into cells located in class 2 (respectively, 1). For cells which are not located at the interface between cells 1 and 2, there is no problem and the classical leap-frog is applied (with the time-step of the class). Note that, as in (13), we replace fields at unknown times by the last known values, denoted * in (16). In Fig. 5 we give the operations proceed in a step of the multi-class Leap-frog method for $N = 3$.

More generally, if we label $LeapFrogH(n, \Delta t)$ (respectively, $LeapFrogE(n, \Delta t)$) the first (respectively, the second) equation of (15) applied to the cells belonging at the class N with a time-step Δt, we can define the multi-class leap-frog method as a recursive process. A step of integration of the recursive leap-frog method is defined by:

$$\begin{cases} 1.\ ComputeH(N, \Delta t), \\ 2.\ ComputeE(N, \Delta t), \end{cases} \tag{17}$$

where the recursive functions $ComputeH(N, \Delta t)$ and $ComputeE(N, \Delta t)$ are respectively defined by:

$$\underline{ComputeH(N, \Delta t)}: \quad \begin{cases} -\ LeapFrogH(N, \Delta t) \\ -\ ComputeH\left(N-1, \frac{\Delta t}{3}\right) \\ -\ ComputeE\left(N-1, \frac{\Delta t}{3}\right) \\ -\ ComputeH\left(N-1, \frac{\Delta t}{3}\right) \end{cases} \qquad \underline{ComputeE(N, \Delta t)}: \quad \begin{cases} -\ LeapFrogE(N, \Delta t) \\ -\ ComputeE\left(N-1, \frac{\Delta t}{3}\right) \\ -\ ComputeH\left(N-1, \frac{\Delta t}{3}\right) \\ -\ ComputeE\left(N-1, \frac{\Delta t}{3}\right) \end{cases}$$

with $ComputeH(1, \delta t)$ defined by $LeapFrogH(1, \delta t)$ and $ComputeE(1, \delta t)$ defined by $LeapFrogE(1, \delta t)$, where δt denotes the time-step.

Since the leap-frog is composed of only two steps (three for the Verlet scheme), this method requires 33% less computation than the Verlet-based recursive scheme, with the same advantages: the scheme is fully explicit, easy to write, does not require additional storage and gives good results with a CPU time significantly reduced. However, we have also the same problems for the stability study as in the Verlet-based method: the CFL must sometimes be strengthened for long-time simulations to ensure stability. From our numerical experience, generally a multiply factor of 0.8 on the time step obtained for non local time-stepping scheme is sufficient to ensure the stability of the local time-stepping scheme.

Various numerical validation results are given in Section 4.3. This local time-stepping method, shows its interests on real problems and gives good comparison results with the two others local time-stepping strategies describe in this paper. The results obtained in this paper are given with a dissipative approach, but similar conclusion would be given for a non-dissipative approach.

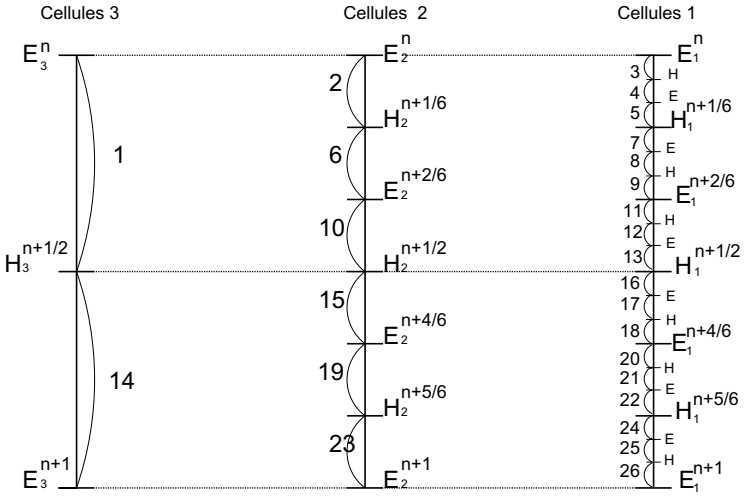

Fig. 5. Steps of recursive leap-frog scheme with three classes.

4.3. Numerical results

In this section, we present some numerical results obtained with the previous local time-stepping methods applied on three different meshes given in Fig. 6. These unstructured meshes, which are typical of problems encountered in industry, contain a large number of cells and present strong cell-size disparities. In these simulations, the aircraft, the space shuttle and the generic missile are all illuminated by a plane wave.

The proposed leap-frog multi-class local time-stepping method (R-LF) has been compared with the 2-class method (2-CL) presented in [8] and the method (R-V) proposed by Piperno. We give in Tables 3–5 the repartition of cells by classes respectively obtained with the three methods. We can notice, for all the methods, the low percentage of small cells, but also important cells-size disparities. For example, there is at least a factor 2^{10} between small and largest cells of the missile mesh (because the R-V scheme uses 10 classes of cells). This explains the real efficiency of multi-class recursive methods on such meshes.

For the three meshes under consideration, Table 6 shows the computational time gain obtained between the standard leap-frog scheme (without local time-stepping) and the three local time-stepping methods discussed in this paper. We first note that the R-LF method is always faster than the other methods. We can also remark that the gain obtained with the 2-CL method is limited whereas, with multi-class methods, the stronger the cell size disparities, the greater the gain in terms of computational time. For example, considering the missile mesh (which presents the most refined unstructured mesh), the improvement obtained with recursive methods is very significant: the R-LF method leads to a scheme 15 times faster than without local time-stepping. In such cases, the requirement of multi-class strategies is clearly highlighted.

On the previous example, the efficiency in terms of CPU-time reduction is clearly shown. In the next example, we propose to study the convergence behaviour of the local time-stepping scheme on a simple case. We take into account the cavity configuration treated in Section 2 and we observe the fields located at the center of this cavity by using different meshes where the local time-stepping strategy is activated or not. To obtain the meshes, we take a regular Cartesian mesh of the cavity with a given spatial step and we refine locally the cells around the center of the cavity. By using this process, we can easily obtain different meshes with different number of classes in the local time-stepping scheme. The first simulations consist to study the behaviour of the scheme when we decrease the time step for fixed spatial meshes. Three meshes have been made to do these simulations. The first mesh is a regular mesh with a spatial size cell equal to 0.2 m and the 2 others have a largest spatial size cell equal to 0.2 m and a smallest size cell respectively equal to 0.1 m and 0.05 m. In the local time-stepping scheme we obtain respectively for the two last meshes a 2-class method and a 3-class method. The errors between the computed and the exact solution are given in Table 7. We note on this table that the convergence behaviour for the scheme with and without local time-stepping is the same. We note also that the errors for the scheme with local time-stepping strategy are smaller than the scheme without local time-stepping strategy. As it has been proved that the scheme without local time-stepping strategy converges, then, the scheme with local time-stepping must converge also.

The second simulations consists to studied the behaviour of the scheme when we increase the number of class in the local time-stepping strategy. From a regular mesh, we divide several times the size of the cells located near the center of the cavity to obtain several meshes which contain until seven class into the local time-stepping scheme. Table 8 shows the different results obtained. We can see in this table that the error do not decrease with the size of the smallest cell. This is not absurd because the error is generally related to the size of the largest cell and this remark is coherent to the results observed in the table. Then, using several classes in local time-stepping seems to do not deteriorate the accuracy of solution. In fact, the error for scheme with local time-stepping strategy is smaller than the scheme without the local time-stepping strategy, then the convergence seems to be ensure also in this case.

We have also compared the DG method using or not the local time-stepping strategy with the FDTD method. Fig. 7 presents on the aircraft example an evaluated scattered component of the field taken at a point outside the aircraft by using the three methods We can see on this figure, the good agreement between the different solutions. In particular, the accuracy of the solution is not altered by using the local time-stepping strategy.

The advantages of using a local time-stepping method are clearly shown for scattering problems, but there remains some difficulties for cavity problems. Indeed, in such cases, long computation time are necessary and

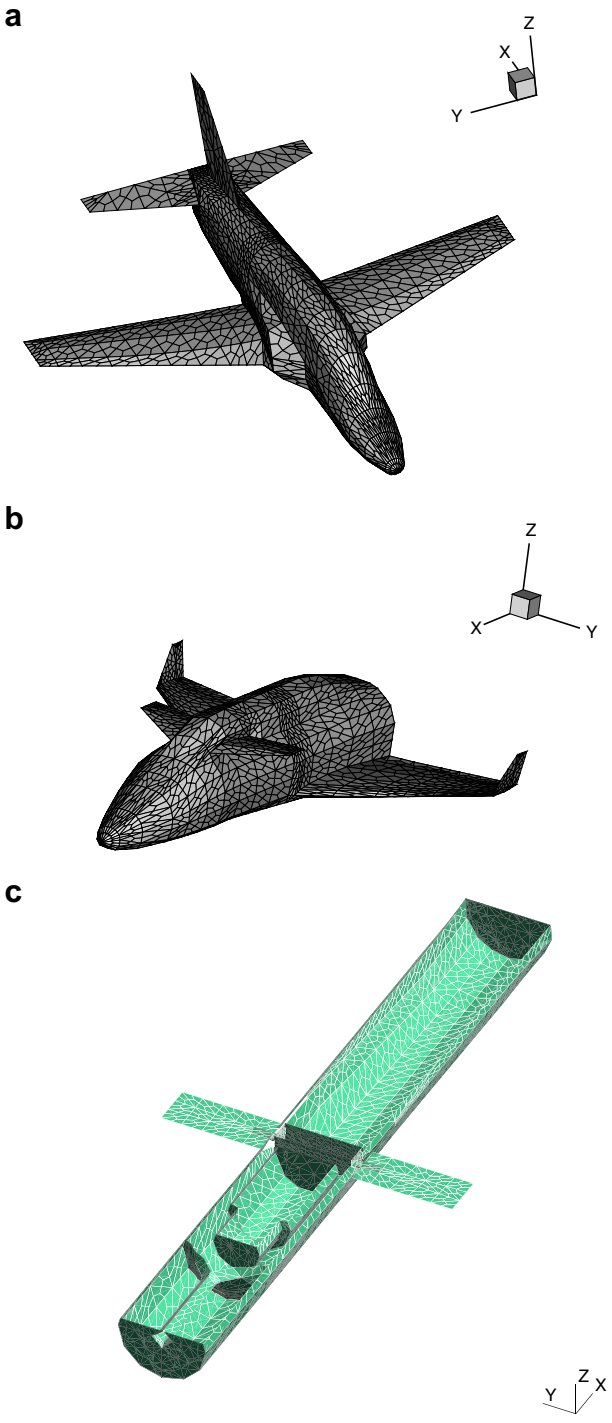

Fig. 6. Meshes considered for comparisons of the different methods: (a) Aircraft, (b) Hermes space shuttle, and (c) Generic missile (opened for display requirements).

we cannot give a stability criteria for the proposed local time-stepping method yet. However, experimental results show that a suitable reduction of the smallest time step (CFL condition) increases the possible observation time and offers the possibility to use the method to treat these kinds of problems in a sufficient time of

Table 3
Cell repartition by classes for the aircraft mesh (~180,000 cells)

Scheme	Class						
	1	2	3	4	5	6	7
2-CL	1000	179,000	×	×	×	×	×
R-LF	1000	16,600	110,400	42,200	8900	×	×
R-V	300	2300	10,800	56,200	67,700	34,000	8700

Table 4
Cell repartition by classes for the shuttle mesh (~105,000 cells)

Scheme	Class					
	1	2	3	4	5	6
2-CL	200	105,200	×	×	×	×
R-LF	100	6600	91,000	7700	×	×
R-V	70	500	4000	38,100	57,300	5500

Table 5
Cell repartition by classes for the missile mesh (~91,000 cells)

Sc	Cl									
	1	2	3	4	5	6	7	8	9	10
2-CL	12	91,000	×	×	×	×	×	×	×	×
R-LF	10	200	1400	14,300	71,600	3500	×	×	×	×
R-V	8	16	160	550	1500	5800	46,000	33,500	3300	200

Table 6
CPU-time gain obtained with different local time-stepping methods versus the leap-frog scheme (without local time-stepping)

Scheme	Mesh		
	Plane	Shuttle	Missile
2-CL	2.5	3.6	2.7
R-V	4.5	4.0	11.0
R-LF	5.5	6.0	15.0

Table 7
Comparison of errors between computed and exact solutions for the DG scheme using or not the local time-stepping strategy

Factor	Regular mesh	2-class mesh	3-class mesh
1	8.06e−3	7.06e−3	6.67e−3
0.5	3.59e−3	2.47e−3	2.20e−3
0.33	2.21e−3	1.41e−3	1.23e−3
0.25	1.52e−3	1.07e−3	8.66e−4
0.2	1.23e−3	8.76e−4	6.66e−4
0.167	1.04e−3	6.66e−4	5.46e−4
0.125	7.83e−4	5.05e−4	4.09e−4
0.0625	4.79e−4	2.80e−4	2.3e−4

The column factor define the value multiplied by the time step. For the regular mesh, we do not use local time-stepping and for the 2-class and 3-class a local time-stepping strategy is employed. For the factor = 1, the time step are $dt = 5.75e-11s$ for the regular mesh and the largest/smallest time steps for the 2-class and 3-class configuration are, respectively, $4.34e-11s/1.44e-11s$ and $3.25e-11s/3.61e-12s$.

observation. For example, considering the cavity problem treated in Section 2, if we strengthen the CFL by a factor 0.8, we obtain a stable solution for a duration time larger than the simulation time generally needed for electromagnetic industrial problems (see Fig. 8). Moreover, despite the reduction of the CFL condition in the

Table 8
Comparison of errors between computed and exact solutions for different number of class in the local time-stepping strategy

Number of class	dt_{max}	dt_{min}	L_2 error	dl_{max} (m)	dl_{min} (m)
1	5.75e−11s	5.75e−11s	8.06e−3	0.2	0.2
2	4.34e−11s	1.44e−11s	7.06e−3	0.2	0.1
3	3.25e−11s	3.61e−12s	6.67e−3	0.2	0.05
4	2.44e−11s	9.02e−13s	4.56e−3	0.2	0.025
6	3.29e−11s	1.35e−13s	6.90e−3	0.2	0.0125
7	2.48e−11s	3.38e−14s	4.82e−3	0.2	0.00625

Columns dt_{min} and dt_{max} define the smallest and the largest time step and columns dl_{min}, dl_{max} define the smallest and the largest spatial cell size.

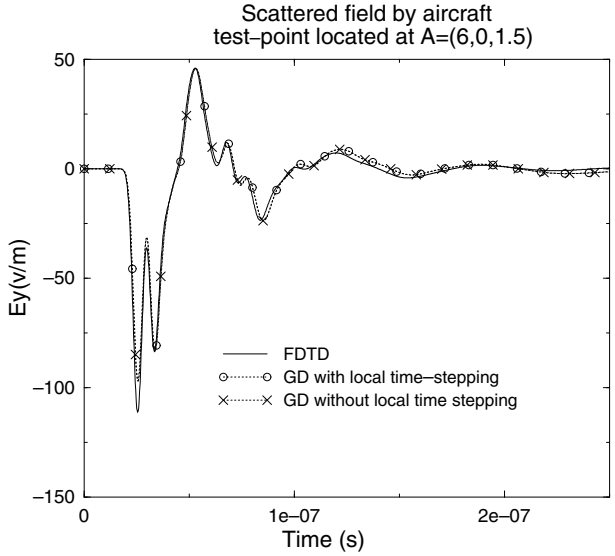

Fig. 7. Comparison of the accuracy of the solution by using or not the local time-stepping method with a Q_2 dissipative spatial approach.

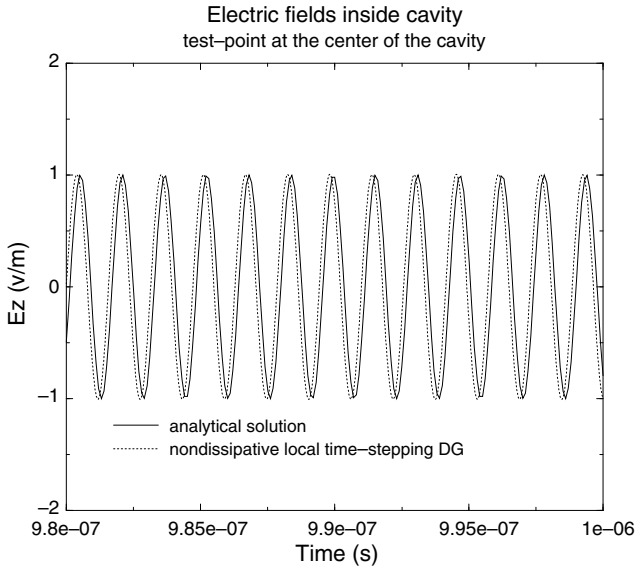

Fig. 8. Field evaluated at the center of a cavity by using the leap-frog multi-class local time-stepping method with a Q_3 non-dissipative spatial approach.

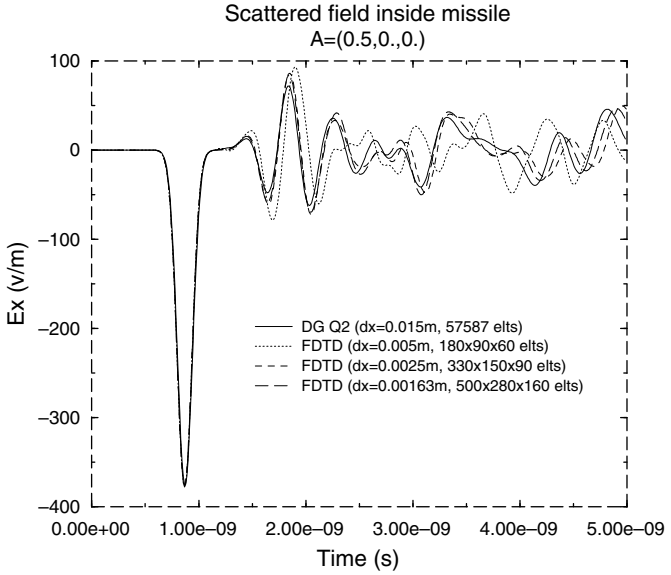

Fig. 9. Comparison of the solution obtained with FDTD and the proposed DG method using a spatial dissipative approach (dx in the DG label defines an average value).

local time-stepping approach, its use in this kind of problems, remains more advantageous in terms of computational time than the FDTD method. Indeed, the dispersive errors due to the FDTD scheme destroys the accuracy of the solution and we need to have very small space step to obtain a correct solution. This constraint implies a small time step and then an important computational time.

Finally, Fig. 9 presents a comparison between the DG method by using the recursive leap-frog local time-stepping strategy, and different FDTD solutions obtained by taking into account different spatial sizes of cells. The quantity under consideration is a scattered field inside the missile illuminated by a plane wave given by $k_y = 1$ and $E_x(t) = 377 * \mathrm{e}^{-((t-2.\mathrm{e}-10)/1.\mathrm{e}-10)^2}$. We can see the advantage to use the DG approach for accuracy and memory storage (reduction by 2 compared to FDTD). However, in terms of CPU-time, despite the use of a local time-stepping strategy for DG, the FDTD remains, in this example, more efficient (two times faster). This is not generally the case but in this example, this is mainly due to the very small size of a few cells in the unstructured mesh. In the future, we can improve this drawback by using in the DG method different spatial approximation orders for each cell. In a such case, the smallest cells will have a low spatial order and an associated time-step larger than the actual local time-stepping strategy. Then the CPU-time for simulations will be reduced.

5. Conclusion

In [8], a non-dissipative Discontinuous Galerkin method using a leap-frog time scheme has been developed to solve time domain Maxwell's equations. This scheme offers real advantages in terms of accuracy and memory storage compared to classical methods like FDTD for problems such as cavity or hight frequency scattering problems. However, on industrial unstructured meshes in which very distorted and/or small cells appear, the DG method can suffer of important spurious modes and a too small time step. This generates a loss in the accuracy of the solution and a CPU-time considerably increased.

In this paper, we proposed and studied the introduction of dissipative penalization terms and an original local time-stepping strategy. It has been proved mathematically and confirmed by means of examples that the dissipative terms provides a new formulation which improves the quality of the solution for distorted meshes and ensures the convergence of our DG scheme for all spatial approximation orders. In particular, we have also the convergence of the order 1 approximation, whereas it was not the case without these penalization

terms. To accelerate the DG method, we propose also a local time-stepping strategy defined by a recursive multi-class method based upon a leap-frog scheme. Some comparisons with other approaches have been done and show the advantages of the proposed method. The statement of an explicit stability condition for this local time-stepping strategy is still an open problem, but numerical examples validated this method and shown that it can be applied without too many restrictions, even for cavity problems. In the future, the local time-stepping methods stay an important stake for Maxwell's equations. In particular other approaches [19] than the methods proposed in this paper could be interesting to investigate.

Other improvements in terms of CPU-time and memory storage of the DG method proposed here will be studied in further works. In particular, considering different spatial approximation orders for each cells and using local time-stepping strategy will imply an additional reduction in CPU-time and memory storage.

Appendix A. Before giving the proofs of Propositions 2 and 3, we assume some background relative to the hexahedral mesh considered here [10]:

- We assume that all hexahedron K are convex and, to characterize an element $K \in \mathcal{T}$, we define the diameter h_K of K and a regularity parameter $\sigma_K = \frac{h_K}{\rho_k}$ where $\rho_K = \|J_{F_K^{-1}}\|_{\infty,K}^{\frac{1}{3}}$ with $J_{F_K^{-1}}$ the determinant of the Jacobian matrix F_K^{-1}.
- We will use the estimates:

$$\begin{aligned} &\|F_K\|_{1,\infty,\widehat{K}} \leqslant Ch_K \quad \text{and} \quad \|J_K\|_{\infty,\widehat{K}} \leqslant Ch_K^3, \\ &\|F_K^{-1}\|_{1,\infty,K} \leqslant C\frac{h_K^2}{\rho_K^3} \quad \text{and} \quad \|J_{F_K^{-1}}\|_{\infty,K} = \rho_K^{-3}, \\ &\lambda((DF_K DF_K^*)(\hat{x})) \leqslant Ch_K^2 \quad \text{and} \quad \lambda((DF_K^{-1} DF_K^{*-1})(\hat{x})) \leqslant C\frac{h_K^4}{\rho_K^6}, \end{aligned} \tag{A.1}$$

where $\lambda(A)$ belongs to the spectrum of A and $C > 0$ is independent of K.

- Finally, we consider a regular family $(\mathcal{T}_h)_{h>0}$ of triangulation of Ω such that when h tends toward 0, it exists a number $\sigma_c > 0$, independent of h, verifying $\forall K \in \mathcal{T}\ \sigma_K \leqslant \sigma_c$.

For the Maxwell equations, we assume also that $\exists \varepsilon_0, \mu_0 > 0$ such that $\forall x \in \Omega$, we have $\varepsilon(x) \geqslant \varepsilon_0$ and $\mu(x) \geqslant \mu_0$. In our analysis, the electric conductivity is $\sigma = 0$.

Proof of Proposition 2. $\forall \psi_h \in \mathbf{V}_r$, the exact solution of the Maxwell equations verifies in particular:

$$\int_K \varepsilon \frac{\partial E}{\partial t} \cdot \psi_h \, dx - \int_K \nabla \times H \cdot \psi_h \, dx = 0 \tag{A.2}$$

and the approximate solution (E_h, H_h):

$$\int_K \varepsilon \frac{\partial}{\partial t} E_h \cdot \psi_h \, dx - \int_K \nabla \times H_h \cdot \psi_h \, dx = \int_{\partial K} (\beta [\![H_h \times n]\!]_{\partial K}^K + \lambda [n \times (E_h \times n)]_{\partial K}^K) \cdot \psi_h \, ds. \tag{A.3}$$

By combining these Eqs. (A.2) and (A.3) and by introducing elements $v_h, w_h \in \mathbf{V}_r$ as $E - E_h = E - v_h + v_h - E_h$ and $H - H_h = H - w_h + w_h - H_h$, we obtain:

$$\begin{aligned} &\int_K \varepsilon \frac{\partial}{\partial t}(E - v_h) \cdot \psi_h \, dx + \int_K \varepsilon \frac{\partial}{\partial t}(v_h - E_h) \cdot \psi_h \, dx - \int_K \nabla \times (H - w_h) \cdot \psi_h \, dx - \int_K \nabla \times (w_h - H_h) \cdot \psi_h \, dx \\ &\quad = \int_{\partial K} (\beta [\![(H_h - w_h) \times n]\!]_{\partial K}^K + \lambda [n \times ((E_h - v_h) \times n)]_{\partial K}^K) \cdot \psi_h \, ds \\ &\qquad + \int_{\partial K} (\beta [\![(w_h - H) \times n]\!]_{\partial K}^K + \lambda [n \times ((v_h - E) \times n)]_{\partial K}^K) \cdot \psi_h \, ds. \end{aligned} \tag{A.4}$$

To obtain the last line of the last expression, we used the fact that $\forall t$, $(E, H)(., t) \in H_0(curl, \Omega) \times H(curl, \Omega)$ ([17]) (i.e. $\forall \Gamma = K \cap K'$, one has $[\![H \times n]\!]_\Gamma^{K \text{or} K'} = [\![E \times n]\!]_\Gamma^{K \text{or} K'} = 0$) and that $\forall \Gamma = K \cap \partial\Omega$, $\beta = 0$ and $E \times n = 0$.

In a same way, one has:

$$\begin{aligned}&\int_K \mu\frac{\partial}{\partial t}(H-w_h)\cdot\phi_h\,\mathrm{d}x+\int_K \mu\frac{\partial}{\partial t}(w_h-H_h)\cdot\phi_h\,\mathrm{d}x+\int_K \nabla\times(E-v_h)\cdot\phi_h\,\mathrm{d}x+\int_K \nabla\times(v_h-E_h)\cdot\phi_h\,\mathrm{d}x\\&\quad=\int_{\partial K}(\gamma[\![(E_h-v_h)\times n]\!]_{\partial K}^K+\lambda[\![n\times((H_h-w_h)\times n)]\!]_{\partial K}^K)\cdot\phi_h\,\mathrm{d}s+\int_{\partial K}(\gamma[\![(v_h-E)\times n]\!]_{\partial K}^K\\&\qquad+\lambda[\![n\times((w_h-H)\times n)]\!]_{\partial K}^K)\cdot\phi_h\,\mathrm{d}s.\end{aligned}\tag{A.5}$$

If one denotes $\Delta_E^P=E-v_h$, $\Delta_E^I=E_h-v_h$, $\Delta_H^P=H-w_h$, $\Delta_H^I=H_h-w_h$ and if one takes $\psi_h=\Delta_E^I$ and $\phi_h=\Delta_H^I$, one obtains:

$$\begin{aligned}&\frac{1}{2}\frac{\mathrm{d}}{\mathrm{d}t}\sum_{K\in\mathcal{T}}\int_K(\varepsilon\Delta_E^I\cdot\Delta_E^I+\mu\Delta_H^I\cdot\Delta_H^I)\mathrm{d}x\\&\leqslant\sum_{K\in\mathcal{T}}\left(\int_K(\varepsilon\frac{\partial}{\partial t}\Delta_E^P\cdot\Delta_E^I+\mu\frac{\partial}{\partial t}\Delta_H^P\cdot\Delta_H^I+\nabla\times\Delta_E^P\cdot\Delta_H^I-\nabla\times\Delta_H^P\cdot\Delta_E^I)\mathrm{d}x\right)\\&\quad+\sum_{K\in\mathcal{T}}\int_{\partial K}(\beta[\![\Delta_H^P\times n]\!]_{\partial K}^K+\lambda[\![n\times(\Delta_E^P\times n)]\!]_{\partial K}^K)\cdot\Delta_E^I\mathrm{d}s\\&\quad+\sum_{K\in\mathcal{T}}\int_{\partial K}(\gamma[\![\Delta_E^P\times n]\!]_{\partial K}^K+\lambda[\![n\times(\Delta_H^P\times n)]\!]_{\partial K}^K)\cdot\Delta_H^I\mathrm{d}s.\end{aligned}\tag{A.6}$$

In the evaluation of the last expression, the choice of β and γ in the DG formalism implies:

$$\sum_{K\in\mathcal{T}}\left(\int_K(\nabla\times\Delta_H^I\cdot\Delta_E^I-\nabla\times\Delta_E^I\cdot\Delta_H^I)\mathrm{d}x-\int_{\partial K}\beta[\![\Delta_H^I\times n]\!]_{\partial K}^K\cdot\Delta_E^I\mathrm{d}s-\int_{\partial K}\gamma[\![\Delta_E^I\times n]\!]_{\partial K}^K\cdot\Delta_H^I\mathrm{d}s\right)=0\tag{A.7}$$

and the choice of $\lambda>0$ implies:

$$\sum_{K\in\mathcal{T}}\left(-\int_{\partial K}\lambda[\![n\times(\Delta_E^I\times n)]\!]_{\partial K}^K\cdot\Delta_E^I\,\mathrm{d}s-\int_{\partial K}\lambda[\![n\times(\Delta_H^I\times n)]\!]_{\partial K}^K\cdot\Delta_H^I\,\mathrm{d}s\right)\leqslant 0.\tag{A.8}$$

We now consider $(v,w)\in\mathbf{V}_r\times\mathbf{V}_r$ such that $\forall(v',w')\in\mathbf{V}_r\times\mathbf{V}_r$ and $\forall K\in\mathcal{T}$,

$$\begin{aligned}&\int_K\varepsilon v\cdot v'\,\mathrm{d}x+\int_K\nabla\times w\cdot v'\,\mathrm{d}x-\int_{\partial K}(\beta[\![w\times n]\!]_{\partial K}^K+\lambda[\![n\times(v\times n)]\!]_{\partial K}^K)\cdot v'\,\mathrm{d}s=l_1(v')\\&\int_K\mu w\cdot w'\,\mathrm{d}x-\int_K\nabla\times v\cdot w'\,\mathrm{d}x-\int_{\partial K}(\gamma[\![v\times n]\!]_{\partial K}^K+\lambda[\![n\times(w\times n)]\!]_{\partial K}^K)\cdot w'\,\mathrm{d}s=l_2(w'),\end{aligned}\tag{A.9}$$

where l_1,l_2 are the two linear forms on $\mathbf{V}_r$ defined by: $l_1(v')=\int_K\varepsilon E\cdot v'\,\mathrm{d}x+\int_K\nabla\times H\cdot v'\,\mathrm{d}x$ and $l_2(w')=\int_K\mu H\cdot w'\,\mathrm{d}x-\int_K\nabla\times E\cdot w'\,\mathrm{d}x$.

Now, if we choose $v_h=v$ and $w_h=w$ solutions of (A.9), and by taking $v'=\Delta_E^I$ and $w'=\Delta_H^I$, we have:

$$\begin{aligned}\sum_{K\in\mathcal{T}}\int_K(\varepsilon\Delta_E^P\cdot\Delta_E^I+\mu\Delta_H^P\cdot\Delta_H^I)\mathrm{d}x&=\sum_{K\in\mathcal{T}}\int_K(\nabla\times\Delta_E^P\cdot\Delta_H^I-\nabla\times\Delta_H^P\cdot\Delta_E^I)\mathrm{d}x\\&\quad+\sum_{K\in\mathcal{T}}\int_{\partial K}(\beta[\![\Delta_H^P\times n]\!]_{\partial K}^K+\lambda[\![n\times(\Delta_E^P\times n)]\!]_{\partial K}^K)\cdot\Delta_E^I\mathrm{d}s\\&\quad+\sum_{K\in\mathcal{T}}\int_{\partial K}(\gamma[\![\Delta_E^P\times n]\!]_{\partial K}^K+\lambda[\![n\times(\Delta_H^P\times n)]\!]_{\partial K}^K)\cdot\Delta_H^I\mathrm{d}s\end{aligned}\tag{A.10}$$

and (A.6) becomes:

$$\begin{aligned}\frac{1}{2}\frac{\mathrm{d}}{\mathrm{d}t}\sum_{K\in\mathcal{T}}\int_K(\varepsilon\Delta_E^I\cdot\Delta_E^I+\mu\Delta_H^I\cdot\Delta_H^I)\mathrm{d}x&\leqslant\sum_{K\in\mathcal{T}}\int_K(\varepsilon\frac{\partial}{\partial t}\Delta_E^P\cdot\Delta_E^I+\mu\frac{\partial}{\partial t}\Delta_H^P\cdot\Delta_H^I)\mathrm{d}x\\&\quad+\sum_{K\in\mathcal{T}}\int_K(\varepsilon\Delta_E^P\cdot\Delta_E^I+\mu\Delta_H^P\cdot\Delta_H^I)\mathrm{d}x.\end{aligned}\tag{A.11}$$

Then, by using Cauchy-Schwartz inequality and the inequalities $\frac{\|\Delta_E^I\|_{0,\varepsilon,\Omega}}{\|(\Delta_E^I,\Delta_H^I)\|_*} \leqslant 1$ and $\frac{\|\Delta_H^I\|_{0,\mu,\Omega}}{\|(\Delta_E^I,\Delta_H^I)\|_*} \leqslant 1$, (A.11) leads to:

$$\frac{\mathrm{d}}{\mathrm{d}t}\|(\Delta_E^I,\Delta_H^I)\|_* \leqslant \|\Delta^P_{\frac{\partial E}{\partial t}}\|_{0,\varepsilon,\Omega} + \|\Delta^P_{\frac{\partial H}{\partial t}}\|_{0,\mu,\Omega} + \|\Delta_E^P\|_{0,\varepsilon,\Omega} + \|\Delta_H^P\|_{0,\mu,\Omega}, \tag{A.12}$$

which concludes the proof. □

Proof of Proposition 3. For this study, we follow the demonstration of [18] but in the non-affine case. In the following, we assume also that C, $\widetilde{C}$, $C_1\ldots$ define generic positive constants which are independent of $h = \max_{K\in\mathcal{T}}(h_K)$.

Let $a : \mathbf{V}_r^2 \times \mathbf{V}_r^2 \to \mathbb{R}$ be the bilinear form defined by:

$$\begin{aligned} a((u,v),(u',v')) = \sum_{K\in\mathcal{T}}\Bigg(&\int_K \varepsilon u\cdot u'\,\mathrm{d}x + \int_K \nabla\times v\cdot u'\,\mathrm{d}x - \int_{\partial K}(\beta[\![v\times n]\!]^K_{\partial K} + \lambda[\![n\times(u\times n)]\!]^K_{\partial K})\cdot u'\,\mathrm{d}s \\ &+ \int_K \mu v\cdot v'\,\mathrm{d}x - \int_K \nabla\times u\cdot v'\,\mathrm{d}x - \int_{\partial K}(\gamma[\![u\times n]\!]^K_{\partial K} + \lambda[\![n\times(v\times n)]\!]^K_{\partial K})\cdot v'\,\mathrm{d}s\Bigg). \end{aligned} \tag{A.13}$$

To prove the Proposition 3, we need essentially to show the continuity and a inf-sup property of the bilinear form a. First, we are going to give a inf-sup property by proving the following result. □

Theorem 2. *There exists $C > 0$ (independent of h) such that*

$$\inf_{(u,v)\in\mathbf{V}_r\times\mathbf{V}_r}\sup_{(u',v')\in\mathbf{V}_r\times\mathbf{V}_r}\frac{a((u,v),(u',v'))}{\|(u,v)\|_h\|(u',v')\|_h} \geqslant C > 0, \tag{A.14}$$

where

$$\|(u,v)\|_h^2 = \|u\|^2_{0,\varepsilon,\Omega} + \|v\|^2_{0,\mu,\Omega} + \|[\![u\times n]\!]\|^2_{0,\mathcal{F}_h} + \|[\![v\times n]\!]\|^2_{0,\mathcal{F}_h} + \sum_{K\in\mathcal{T}} h_K(\|\nabla\times u\|^2_{0,K} + \|\nabla\times v\|^2_{0,K})$$

and where $\mathcal{F}_h$ denotes the set of faces of $\mathcal{T}$ and

$$\|[\![u\times n]\!]\|^2_{0,\mathcal{F}_h} = \sum_{\Gamma=K\cap K'}\int_\Gamma \|u_{K'}\times n_K - u_K\times n_K\|^2 ds + \sum_{\Gamma=K\cap\partial\Omega}\int_\Gamma \|u_K\times n_K\|^2 ds.$$

To prove this result, we begin to demonstrate three propositions on the overestimations of the different terms of the bilinear form a. We choose test-functions u' and v' such that $u'\circ F_K = DF_K^{*-1}\hat{\nabla}\times\hat{v} = DF_K^{*-1}\hat{u}'$ and $v'\circ F_K = -DF_K^{*-1}\hat{\nabla}\times\hat{u} = DF_K^{*-1}\hat{v}'$. The first proposition gives a overestimation of the terms of order 1 in the bilinear form a:

Proposition 4. *It exists $C > 0$ (independent of h) such that*:

$$\|u'\|_{0,\Omega} \leqslant C\|v\|_{0,\Omega} \text{ and } \|v'\|_{0,\Omega} \leqslant C\|u\|_{0,\Omega}. \tag{A.15}$$

Proof of Proposition 4.

$$\begin{aligned} \|u'\|_{0,K} &= \int_{\widehat{K}} |J_K| u'\circ F_K\cdot u'\circ F_K \mathrm{d}\hat{x} = \int_{\widehat{K}} |J_K| DF_K^{*-1}\hat{\nabla}\times\hat{v}\cdot DF_K^{*-1}\hat{\nabla}\times\hat{v}\mathrm{d}\hat{x} \leqslant Ch_K\int_{\widehat{K}}\hat{\nabla}\times\hat{v}\cdot\hat{\nabla}\times\hat{v}\mathrm{d}\hat{x} \\ &\leqslant C'h_K\int_{\widehat{K}}\hat{v}\cdot\hat{v}\mathrm{d}\hat{x} \quad \text{since } \hat{v}\in[\mathcal{Q}_r(\widehat{K})]^3 \leqslant C'h_K\int_{\widehat{K}}\frac{|J_K|}{|J_K|}(DF_K^*DF_K^{*-1})\hat{v}\cdot(DF_K^*DF_K^{*-1})\hat{v}\mathrm{d}\hat{x} \leqslant C''\|v\|_{0,K}. \end{aligned}$$

We have used (A.1) to obtain these estimates. The second estimate of the proposition is obtained by the same process. The second proposition concerns the underestimation of curl-terms in the bilinear form a: □

Proposition 5. *It exists $C > 0$ (independent of h) such that*:

$$-(\nabla_h \times u, v')_{0,\Omega} = -\sum_{K\in\mathcal{T}} \int_K \nabla \times u \cdot v' \, dx \geqslant C \sum_{K\in\mathcal{T}} h_K \|\nabla \times u\|^2_{0,K}$$

$$(\nabla_h \times v, u')_{0,\Omega} = \sum_{K\in\mathcal{T}} \int_K \nabla \times v \cdot u' \, dx \geqslant C \sum_{K\in\mathcal{T}} h_K \|\nabla \times v\|^2_{0,K}.$$

Proof of Proposition 5.

$$\begin{aligned}
-(\nabla_h \times u, v')_{0,\Omega} &= -\sum_{K\in\mathcal{T}_h} (\nabla \times u, v')_{0,K} = -\sum_{K\in\mathcal{T}} \int_{\widehat{K}} \hat{\nabla} \times \hat{u}_K \cdot \hat{v}'_K \, \mathrm{d}\hat{x} = \sum_{K\in\mathcal{T}} \int_{\widehat{K}} \hat{\nabla} \times \hat{u}_K \cdot \hat{\nabla} \times \hat{u}_K \mathrm{d}\hat{x} \\
&= \sum_{K\in\mathcal{T}} \int_{\widehat{K}} \frac{|J_K|}{|J_K|} \left(J_K DF_K^{*-1} \frac{DF_K^*}{J_K} \right) \hat{\nabla} \times \hat{u}_K \cdot \left(J_K DF_K^{*-1} \frac{DF_K^*}{J_K} \right) \hat{\nabla} \times \hat{u}_K \mathrm{d}\hat{x} \\
&\geqslant C \sum_{K\in\mathcal{T}} h_K \|\nabla \times u\|^2_{0,K}.
\end{aligned}$$

We have used (A.1) to obtain these estimates. The second estimate of the proposition is obtained by the same process. The third proposition concerns the jump terms of the bilinear form a: □

Proposition 6. *It exists $C > 0$ (independent of h) such for all $\delta_1, \delta_2, \delta_3, \delta_4 \in \mathbb{R}^*$, we have*:

$$\sum_{K\in\mathcal{T}} \int_{\partial K} \beta [\![v \times n]\!]^K_{\partial K} \cdot u' \, ds \leqslant C \left(\delta_1^2 \| [\![v \times n]\!] \|^2_{0,\mathcal{F}_h^i} + \frac{1}{\delta_1^2} \sum_{K\in\mathcal{T}} h_K \|\nabla \times v\|^2_{0,K} \right)$$

$$\sum_{K\in\mathcal{T}} \int_{\partial K} \lambda [\![n \times (u \times n)]\!]^K_{\partial K} \cdot u' \, ds \leqslant C \left(\delta_2^2 \| [\![u \times n]\!] \|^2_{0,\mathcal{F}_h} + \frac{1}{\delta_2^2} \sum_{K\in\mathcal{T}_h} h_K \|\nabla \times v\|^2_{0,K} \right)$$

$$\sum_{K\in\mathcal{T}} \int_{\partial K} \lambda [\![n \times (v \times n)]\!]^K_{\partial K} \cdot v' \leqslant C \left(\delta_3^2 \| [\![v \times n]\!] \|^2_{0,\mathcal{F}_h} + \frac{1}{\delta_3^2} \sum_{K\in\mathcal{T}_h} h_K \|\nabla \times u\|^2_{0,K} \right)$$

$$\sum_{K\in\mathcal{T}} \int_{\partial K} \gamma [\![u \times n]\!]^K_{\partial K} \cdot v' \, ds \leqslant C \left(\delta_4^2 \| [\![u \times n]\!] \|^2_{0,\mathcal{F}_h} + \frac{1}{\delta_4^2} \sum_{K\in\mathcal{T}} h_K \|\nabla \times u\|^2_{0,K} \right).$$

Proof of Proposition 6. We only prove the first inequality. One obtains the others by using the same technique. Using the Cauchy-Schwarz inequality, we can write:

$$\sum_{K\in\mathcal{T}} \int_{\partial K} \beta [\![v \times n]\!]^K_{\partial K} \cdot u' \, \mathrm{d}s \leqslant \sum_{K\in\mathcal{T}} \| \beta [\![v \times n]\!]^K_{\partial K} \|_{0,\partial K} \|u'\|_{0,\partial K} \tag{A.16}$$

Let $\delta_1 \neq 0$. By using $(\delta_1 a - \frac{b}{\delta_1})^2 = \delta_1^2 a^2 + \frac{b^2}{\delta_1^2} - 2ab \geqslant 0$ $(a, b \in \mathbb{R})$, (A.16) leads to:

$$\sum_{K\in\mathcal{T}} \int_{\partial K} \beta [\![v \times n]\!]^K_{\partial K} \cdot u' \, \mathrm{d}s \leqslant \sum_{K\in\mathcal{T}} \left(\frac{\delta_1^2}{2} \| \beta [\![v \times n]\!]^K_{\partial K} \|^2_{0,\partial K} + \frac{1}{2\delta_1^2} \|u'\|^2_{0,\partial K} \right). \tag{A.17}$$

We have also [10] $\forall u \in \mathbf{V}_r$ and $K \in \mathcal{T}$, it exists $C > 0$ (independent of K) such that $\|u_{|K}\|_{0,\partial K} \leqslant \frac{C}{h_K} \|u\|_{0,K}$. So, (A.17) becomes:

$$\sum_{K\in\mathcal{T}} \int_{\partial K} \beta [\![v \times n]\!]^K_{\partial K} \cdot u' \, \mathrm{d}s \leqslant \sum_{K\in\mathcal{T}} \left(\frac{\delta_1^2}{2} \| \beta [\![v \times n]\!]^K_{\partial K} \|^2_{0,\partial K} + \frac{C}{2\delta_1^2 h_K} \|u'\|^2_{0,K} \right). \tag{A.18}$$

Finally, the definition of u' gives $\|u'\|^2_{0,K} \leqslant C h_K^2 \|\nabla \times v\|_{0,K}$ (for a certain constant $C > 0$) and then, by using (A.18), we complete the proof. □

By using the Proposition 5, we have:

$$a((u,v),(u',v')) - \sum_{K\in\mathcal{T}}\left(\int_K(\varepsilon u\cdot u' + \mu v\cdot v')\mathrm{d}x + \int_{\partial K}(\beta[\![v\times n]\!]_{\partial K}^K + \lambda[\![n\times(u\times n)]\!]_{\partial K}^K)\cdot u'\,\mathrm{d}s\right.$$
$$\left. + \int_{\partial K}(\gamma[\![u\times n]\!]_{\partial K}^K + \lambda[\![n\times(v\times n)]\!]_{\partial K}^K)\cdot v'\,\mathrm{d}s\right)$$
$$= \sum_{K\in\mathcal{T}}\int_K(-\nabla\times u\cdot v' + \nabla\times v\cdot u')\mathrm{d}x \geqslant C\sum_{K\in\mathcal{T}}h_K(\|\nabla\times v\|_{0,K}^2 + \|\nabla\times u\|_{0,K}^2).$$

By using the Proposition 4, it exists a constant $C>0$ such that

$$\int_K(\varepsilon u\cdot u' + \mu v\cdot v')\mathrm{d}x \leqslant C(\|u\|_{0,\varepsilon,\Omega}^2 + \|v\|_{0,\mu,\Omega}^2). \tag{A.19}$$

By using the Proposition 6, we find a constant $C>0$ such that for all $\delta_1,\delta_2,\delta_3,\delta_3\neq 0$, we have:

$$\sum_{K\in\mathcal{T}}\left(\int_{\partial K}(\beta[\![v\times n]\!]_{\partial K}^K + \lambda[\![n\times(u\times n)]\!]_{\partial K}^K\right)\cdot u'\,\mathrm{d}s + \int_{\partial K}(\gamma[\![u\times n]\!]_{\partial K}^K + \lambda[\![n\times(v\times n)]\!]_{\partial K}^K)\cdot v'\,\mathrm{d}s)$$
$$\leqslant C(\delta_1^2+\delta_3^2)\|[\![v\times n]\!]\|_{0,\mathcal{F}_h}^2 + C(\delta_2^2+\delta_4^2)\|[\![u\times n]\!]\|_{0,\mathcal{F}_h}^2 + C\left(\frac{1}{\delta_1^2}+\frac{1}{\delta_2^2}\right)\sum_{K\in\mathcal{T}}h_K\|\nabla\times v\|_{0,K}^2$$
$$+ C\left(\frac{1}{\delta_3^2}+\frac{1}{\delta_4^2}\right)\sum_{K\in\mathcal{T}}h_K\|\nabla\times u\|_{0,K}^2. \tag{A.20}$$

Finally, by taking into account (A.19) and (A.20), one can always choose $\delta_1,\delta_2,\delta_3,\delta_4$ such that: $\exists C,\widetilde{C}>0$

$$C\sum_{K\in\mathcal{T}}h_K(\|\nabla\times v\|_{0,K}^2 + \|\nabla\times u\|_{0,K}^2) \leqslant a((u,v),(u',v')) + \widetilde{C}(\|u\|_{0,\varepsilon,\Omega}^2 + \|v\|_{0,\mu,\Omega}^2 + \|[\![u\times n]\!]\|_{0,\mathcal{F}_h}^2$$
$$+ \|[\![v\times n]\!]\|_{0,\mathcal{F}_h}^2) = a((u,v),(u',v')) + \widetilde{C}a((u,v),(u,v)). \tag{A.21}$$

By adding the term $C(\|u\|_{0,\varepsilon,\Omega}^2 + \|v\|_{0,\mu,\Omega}^2 + \|[\![u\times n]\!]\|_{0,\mathcal{F}_h}^2 + \|[\![v\times n]\!]\|_{0,\mathcal{F}_h}^2)$ to the previous inequality, we obtain:

$$C\|(u,v)\|_h^2 \leqslant a((u,v),(u'+C_1u,v'+C_1v)), \tag{A.22}$$

where $C_1 = C+\widetilde{C}$.

Now, we are going to prove that $\|(u',v')\|_h \leqslant C\|(u,v)\|_h$. By using Proposition 4, we obtain:$\|u'\|_{0,\varepsilon,\Omega}\leqslant C\|v\|_{0,\mu,\Omega}$ and $\|v'\|_{0,\mu,\Omega}\leqslant C\|u\|_{0,\varepsilon,\Omega}$.By using (A.1), we have:

$$\|\nabla\times u'\|_{0,K}^2 \leqslant \frac{C}{h_K}\|\hat{\nabla}\times\hat{u'}\|_{0,\widehat{K}}^2 \leqslant \frac{C'}{h_K}\|\hat{u'}\|_{0,\widehat{K}}^2 \text{ because} u'\in[Q_r(\widehat{K})]^3 \leqslant \frac{C'}{h_K}\|\hat{\nabla}\times\hat{v}\|_{0,\widehat{K}}^2 \leqslant C''\|\nabla\times v\|_{0,K}^2$$

and

$$\|\nabla\times v'\|_{0,K}^2 \leqslant C\|\nabla\times u\|_{0,K}^2.$$

Moreover, we can prove:

$$\|[\![u'\times n]\!]\|_{0,\mathcal{F}_h}^2 \leqslant C\sum_{K\in\mathcal{T}}h_K\|\nabla\times v\|_{0,K}$$

and

$$\|[\![v'\times n]\!]\|_{0,\mathcal{F}_h}^2 \leqslant C\sum_{K\in\mathcal{T}}h_K\|\nabla\times u\|_{0,K}.$$

Indeed, it is easy to see that

$$\|[\![u' \times n]\!]\|^2_{0,\mathcal{F}_h} \leqslant \sum_{K\in\mathcal{T}} \int_{\partial K} \|u'_K \times n_K\|^2 \mathrm{d}s \leqslant \sum_{K\in\mathcal{T}} \int_{\partial K} \|u'_K\|^2 \mathrm{d}s \tag{A.23}$$

Now, by using (A.1), it exists a constant C such that:

$$\sum_{K\in\mathcal{T}} \int_{\partial K} \|u'_K\|^2 \mathrm{d}s \leqslant C \sum_{K\in\mathcal{T}} h_K \int_K \nabla \times v \cdot \nabla \times v \mathrm{d}x$$

which gives the expected result. Finally, if we take $(w_1, w_2) = (u' + C_1 u, v' + C_1 v) \in \mathbf{V}_r \times \mathbf{V}_r$, (A.22) leads to

$$C\|(u,v)\|_h \|(w_1,w_2)\|_h \leqslant a((u,v),(w_1,w_2)),\ \forall (u,v) \in \mathbf{V}_r \times \mathbf{V}_r$$

for a certain constant $C > 0$ independent of h. So, we obtain the inf-sup condition (A.14). The next step of the demonstration of the Proposition 3 is to verify the continuity of the bilinear form a. To obtain this result, you have the following lemma:

Lemma 1. *It exists $M > 0$ (independent of h) such that*

$$a((u,v),(u',v')) \leqslant M\|(u,v)\|_{h,\frac{1}{2}} \|(u',v')\|_h, \quad \forall u, v, u', v' \in \mathbf{V}_r$$

where $\|(u,v)\|^2_{h,\frac{1}{2}} = \|(u,v)\|^2_h + \sum_{K\in\mathcal{T}} (h_K^{-1}(\|u\|^2_{0,K} + \|v\|^2_{0,K}) + \|u\|^2_{0,\partial K} + \|v\|^2_{0,\partial K})$.

To verify this lemma, it is sufficient to integrate by parts $a((u,v),(u',v'))$ (For more detail see [18]).

Recall that we solve the problem: find $(u,v) \in \mathbf{V}_r \times \mathbf{V}_r$ such that $\forall (u',v') \in \mathbf{V}_r \times \mathbf{V}_r$, $a((u,v),(u',v')) = (l_1(u'), l_2(v'))$. So, we have immediately the consistency result: $a((u-E, v-H),(u',v')) = 0$ for all (u',v') in $\mathbf{V}_r \times \mathbf{V}_r$. Now the inf-sup condition and the continuity of the bilinear form lead to the well-known estimate:

$$\|(u-E, v-H)\|_h \leqslant C \inf_{(u',v')\in \mathbf{V}_r \times \mathbf{V}_r} \|(E-u', H-v')\|_{h,\frac{1}{2}}$$

for a certain constant $C > 0$. In [10], we have derived for a particular projector π_h the following interpolations error: let $v \in [H^{s+1}(K)]^3$ with $s \geqslant 0$ a real. There exists a constant $C > 0$ independent of h such that

$$\|v - \pi_{h|K} v\|_{0,K} \leqslant C h_K^{\min(s,r)} \|v\|_{s+1,K}$$

$$|v - \pi_{h|K} v|_{1,K} \leqslant C h_K^{\min(s-1,r-1)} \|v\|_{s+1,K}$$

$$\|(v - \pi_{h|K} v) \times n_K\|_{0,\partial K} \leqslant C h_K^{\min(s-\frac{1}{2}, r-\frac{1}{2})} \|v\|_{s+1,K}.$$

So, If we assume that the exact solution verifies $(E,H) \in H^{s+1}(\mathcal{T})$ for $s \geqslant 0$, then there exists a constant $C > 0$ such that:

$$\|u-E, v-H\|_* \leqslant \|(u-E, v-H)\|_h \leqslant C h^{\min(s-\frac{1}{2}, r-\frac{1}{2})} \max(\|E\|_{s+1,h}, \|H\|_{s+1,h})$$

where $H^s(\mathcal{T}) = \{v \in [L^2(\Omega)]^3 : \forall K \in \mathcal{T},\ v_{|K} \in [H^s(K)]^3\}$ and $\|v\|^2_{s,h} = \sum_{K\in\mathcal{T}} \|v\|^2_{s,K}$ and the Proposition 3 is verified.

References

[1] Andreas C. Cangellaris, Diana B. Wright, Analysis of the numerical error caused by the stair-stepped approximation of a conducting boundary in FDTD simulations of electromagnetic phenomena, IEEE Trans. Antennas Prop. AP-39 (10) (1991) 1518–1525.

[2] K.S. Yee, Numerical solution of initial boundary value problems involving Maxwell's equation in isotropic media, IEEE Trans. Antennas Prop. 14 (3) (1966) 302–307.

[3] A. Taflove, S.C. Hagness, Computational Electrodynamics: The Finite-Difference Time-Domain Method, second ed., Artech, Norwood, MA.

[4] P. Bonnet, X. Ferrieres, Numerical modeling of scattering problems using a time domain finite volume method, JEMWA 11 (1997) 1165–1189.

[5] S. Piperno, M. Remaki, L. Fezoui, A non-diffusive finite volume scheme for the 3D Maxwell equations on unstructured meshes, SIAM J. Numer. Anal. 39 (6) (2002) 2089–2108.

[6] F. Edelvik, G. Ledfelt, Explicit hybrid time domain solver for the Maxwell equations in 3D, J. Sci. Comput. 15 (1) (2000).

[7] J.S. Hesthavens, T. Warburton, High-order Nodal methods on unstructured grids. I. Time-domain solution of Maxwell's equations, J. Comput. Phys. 181 (2002) 1–34.
[8] G. Cohen, X. Ferriéres, S. Pernet, A spatial high order hexahedral Discontinuous Galerkin method to solve Maxwell's equations in time domain, J. Comput. Phys. 217 (2006) 340–363.
[9] G. Cohen, M. Duruflé, Nonspurious spectral-like element methods for Maxwell's equations, J. Comp. Math. 25 (2007) 282–304.
[10] S. Pernet, X. Ferrieres, HP – a priori error estimates for a non-dissipative spectral Discontinuous Galerkin method to solve the Maxwell equations in the time domain, Math. Comp. 76 (2007) 1801–1832.
[11] J.-P. Berenger, A perfectly matched layer for the absorption of electromagnetic waves, J. Comput. Phys. 114 (1994) 185–200.
[12] J. -C Nédélec, Mixed finite elements in $\mathbb{R}^3$, Numer. Math. 35 (3) (1980) 315–341.
[13] S. Pernet, Etude de méthodes d'ordre élevé pour résoudre les équations de Maxwell dans le domaine temporel. application à la détection et à la compatibilité électromagnétique, Doctorat de mathématiques appliquées de l'Université Dauphine-Paris IX, 2004.
[14] F. Collino, T. Fouquet, P. Joly, Conservative space-time mesh refinement methods for the FDTD solution of Maxwell's equation, J. Comput. Phys. 211 (2006) 9–35.
[15] S. Piperno, Symplectic local time-stepping in non-dissipative DGTD methods applied to wave propagation problems, M2AN 40 (5) (2006) 815–841.
[16] P. Nettesheim, S. Reich, Symplectic multiple-time-stepping integrators for quantum-classical molecular dynamics, Lect. Notes Comput. Sci. Eng. 4 (1998) 412–420.
[17] M. Remaki, Méthodes numériques pour les equations de Maxwell instationnaires en milieu hétérogène, Doctorat de mathématiques appliquées de l'Ecole Nationale des Ponts et Chaussées, 1999.
[18] A. Ern, J.-L. Guermond, Discontinuous Galerkin methods for Friedrichs' systems. I. General theory, SIAM J. Numer. Anal. 44 (2) (2006) 753–778.
[19] M. Dumbser, M. Kaser, E.F. Toro, An arbitrary high order Discontinuous Galerkin method for elastic waves on unstructured meshes V: Local time stepping and p-adaptivity, Geophys. J. Int. (2000) 142.
[20] J.S. Hesthaven, T. Warburton, High order Nodal Discontinuous Galerkin methods for the Maxwell eigenvalue problem, R. Soc. Lond. Ser. A 362 (2004) 493–524.
[21] M. Ainsworth, Dispersive and dissipative behaviour of high order Discontinuous Galerkin finite element methods, J. Comp. Phys. 198 (2004) 106–130.